Check for updates

JGR Earth Surface

RESEARCH ARTICLE
10.1029/2023JF007080

Special Section:
Prediction in coastal geomorphology

Exploring Controls on Coastal Dune Growth Through a Simplified Model

Katerina Kombiadou[1], Susana Costas[1], and Dano Roelvink[2]

[1]Centre for Marine and Environmental Research (CIMA)—Infrastructure Network in Aquatic Research (ARNET), Faculty of Science and Technology, University of Algarve, Faro, Portugal, [2]Water Science and Engineering Department, IHE Delft Institute for Water Education, Delft, the Netherlands

Key Points:

- Duna morphodynamic model is calibrated and validated against Computational Fluid Dynamics model results and field data
- The influence of dune shape (height and slope), wind incidence, vegetation density and beach width on dune growth is investigated
- Dune height and plant cover are the main factors controlling accumulation patterns, sand recycling and vertical growth

Supporting Information:

Supporting Information may be found in the online version of this article.

Correspondence to:

K. Kombiadou,
akompiadou@ualg.pt

Citation:

Kombiadou, K., Costas, S., & Roelvink, D. (2023). Exploring controls on coastal dune growth through a simplified model. *Journal of Geophysical Research: Earth Surface*, *128*, e2023JF007080. https://doi.org/10.1029/2023JF007080

Received 27 JAN 2023
Accepted 3 AUG 2023

Author Contributions:

Conceptualization: Susana Costas
Data curation: Katerina Kombiadou, Susana Costas
Formal analysis: Katerina Kombiadou
Funding acquisition: Susana Costas
Investigation: Katerina Kombiadou, Susana Costas
Methodology: Susana Costas, Dano Roelvink
Project Administration: Susana Costas

© 2023 The Authors.
This is an open access article under the terms of the Creative Commons Attribution-NonCommercial License, which permits use, distribution and reproduction in any medium, provided the original work is properly cited and is not used for commercial purposes.

Abstract Process-based morphodynamic models can be useful in understanding coastal dune responses to disturbances, as well as possible evolutionary patterns. To this aim, we employ Duna, a simplified 1D morphodynamic model, to assess the influence of dune morphology (height and slope) on sand transfer and deposition across the dune profile for different beach widths and wind incidence angles through idealized experiments. Simulations of real conditions show good model performance, both in wind flow reproduction and in topographic change along the dune profiles tested. The idealized experiments show that wind speed increases and sand accumulation decreases logarithmically with dune height and linearly with stoss slope along the dune profile. Fetch and cosine transport limiting parameters are reflected in the sand accumulated windwards from the toe, while sand transfer to the dune appears controlled by multiple factors; the higher the dune and/or the narrower the beach, the likelier that maximum accumulation occurs under oblique winds. Results point to two different types of evolution for high dunes. Either the vegetation is dense enough to maintain the stoss position, in which case vertical growth near-ceases and seaward progradation is promoted, or the stoss is eroded and landward retreat dominates, in which case sand transfer to the crest and lee continues as a mixture of low input from the beach and recycled sand from the stoss.

Plain Language Summary Coastal dunes are sensitive ecosystems whose survival depends on their adaption to changing conditions. Thus, it is important to understand how dune characteristics (i.e., shape, vegetation type, and cover) and prevailing conditions (i.e., wind speed and direction, beach width) determine where and when sand is deposited onto the dune, promoting growth. This is the result of a complex balance between winds that bring sand to the dune from the adjacent beach (main sand provider), the dune topography (decelerating winds near the dune toe and accelerating them along the slope, up to the dune crest) and dune plants (slowing winds down in their vicinity and trapping wind-blown sand). The main controls on these complex interactions have been incorporated into the Duna model for aeolian sand transport. After tuning parameters and verifying that simulated results are accurate, Duna is used to assess the impacts of dune shape (height and slope), beach width, vegetation coverage and wind angles to wind flow and topographic changes on the dune. Results show that both wind speed and sand accumulation vary logarithmically with dune height and linearly with slope. The simulated sand distribution along the dune is used as a basis to draw generalized dune growth patterns.

1. Introduction

Coastal dunes, lying at the interface between ocean and land, are fragile and complex systems regulated by biotic (e.g., plants, animals, biotic crusts, etc.) and abiotic factors (e.g., sediment, wind and nutrient fluxes, precipitation, etc.) and their multiple interactions (Brodie et al., 2019; Costas et al., 2023; Durán Vinent & Moore, 2015; Stallins & Corenblit, 2018). Their importance as ecosystem service providers has been widely acknowledged, motivating research on the different aspects controlling the evolution of these systems, such as vegetation cover (e.g., Talavera et al., 2022), dune shape, beach state (e.g., Garzon et al., 2022) and the processes controlling dynamics over distinct temporal scales, from event-scale (e.g., Costas et al., 2020) to multi-decadal (e.g., Herrero et al., 2020) changes. Coastal dunes display not only significant morphological variability alongshore (Houser, 2013; Houser et al., 2018; Moore et al., 2018), but also variable response depending on the shoreline trends at the adjacent beach (Brodie et al., 2019; Houser et al., 2022). Dune shape (i.e., aspect ratio or ratio between the height and width) has been suggested to influence storm-induced dune erosion (Itzkin et al., 2020), while dune height has been traditionally used to assess the impact of storms at sandy coasts (Ferreira et al., 2016;

21699011, 2023, 9, Downloaded from https://agupubs.onlinelibrary.wiley.com/doi/10.1029/2023JF007080 by Cochrane Portugal, Wiley Online Library on [06/11/2023]. See the Terms and Conditions (https://onlinelibrary.wiley.com/terms-and-conditions) on Wiley Online Library for rules of use; OA articles are governed by the applicable Creative Commons License

Software: Katerina Kombiadou, Dano Roelvink
Supervision: Susana Costas, Dano Roelvink
Validation: Katerina Kombiadou, Susana Costas, Dano Roelvink
Visualization: Katerina Kombiadou
Writing – original draft: Katerina Kombiadou
Writing – review & editing: Katerina Kombiadou, Susana Costas, Dano Roelvink

Sallenger, 2000). However, the relative importance of the factors controlling dune shape and their impact on foredune growth is understudied (Hovenga et al., 2023).

Durán and Moore (2013), based on ecomorphodynamic model simulations forced with constant onshore winds, introduced the idea that foredunes are scale invariant, with long-term growth being limited by a negative feedback between wind flow and topography, and with vegetation type controlling the maximum dune height. Based on field data, R. Davidson-Arnott et al. (2018) opposed the hypothesis of an equilibrium dune height and postulated that stoss slope steepness cannot limit sand transfer to a halt as much of the dune vertical growth takes place under oblique winds. Recent research by Schwarz et al. (2021) also highlights the importance of wind direction and vegetation cover to foredune growth and recovery. On one hand, this research relates sediment flux limitation at the dune toe to fetch-induced sediment availability, which in turn may be controlled by wind direction (Bauer & Davidson-Arnott, 2003; Delgado-Fernandez, 2010; Walker et al., 2009). On the other hand, it relates sediment flux limitation at the dune crest to transport capacity, which the authors suggest is determined by the wind velocity and the distance traveled over vegetation. Wind velocity was found to accelerate from the dune foot to the crest, in particular for shore-perpendicular winds (Arens et al., 1995; Schwarz et al., 2021; Walker et al., 2017). Schwarz et al. (2021) suggest that dune height and stoss slope, which, together with wind direction, control the magnitude of wind acceleration across the dune slope, could play a critical role in foredune growth and recovery after storm-derived erosion. In this regard, and despite having explored only one large dune, the authors suggest that, due to differences in topographic steering, growth capacity at the crest differs between low and high foredunes. In the former case, shore-parallel and weak oblique winds induce similar growth, while in the latter case, vertical growth is favored during oblique winds.

The complex interactions between ecological and geomorphological aeolian processes and the influence of nearshore sediment transport governing coastal dune morphodynamics have inspired the development of numerical models that aim to address these complexities and resolve the dynamics at different spatiotemporal scales (Keijsers et al., 2016). The main interactions between wind, sand transport and dune vegetation are described in most models, with variable degree of detail (i.e., depending on the focus and the timescale of the simulation, processes often can be simplified or omitted), using process-based, semiempirical and/or statistical methods, or a combination thereof (Roelvink & Costas, 2019).

In terms of wind flow, computational fluid dynamics (CFD) modeling has enabled to reproduce highly detailed and complex airflow patterns and their dependencies on coastal dune morphology (Hesp & Smyth, 2016, 2021; Hesp et al., 2015; Jackson et al., 2011; Parsons et al., 2004; Smith et al., 2017). However, the computational cost involved, to date, inhibits the use of CFD models for morphodynamics. Instead, coastal morphodynamic models use more simplified (1D or 2D) wind flow solutions that cannot reproduce all the complexities associated with wind-topography interaction. Still, such models appear to fairly represent fundamental processes (Cohn et al., 2019; Costas et al., 2019; Roelvink & Costas, 2019) while maintaining the required simplicity to enable longer-term simulations. In fact, models that explicitly describe morphodynamic processes when applied at medium to long scales incorporate shorter scale changes (e.g., beach erosion and recovery), thus providing a means to integrate transport between scales.

In terms of coastal dune morphological change, categorizing models is not straightforward due to differences in model complexity (incorporated processes and interactions) and spatiotemporal scales of change described. Still, models can be broadly grouped under two main categories: data-driven and process-based. To simulate the complex processes governing coastal dune change, data-driven models often employ statistical and semiempirical expressions and/or learning algorithms (i.e., genetic, or neural networks), while process-based models employ analytic expressions and numerical methods. DOONIES (Charbonneau et al., 2022) is a stochastic, grid-based ecogeomorphic community model for coastal dune vegetation, incorporating biological, physiological, and geomorphological drivers. Statistical approaches, such as cellular automaton (CA) models or genetic programming (GP), that describe complex interactions using probabilistic rules have also been developed. For example, DUBEVEG (Keijsers et al., 2016) uses CA to describe crucial bio-physical feedback interactions for dune growth, development and decay and the CA model of Poppema et al. (2022) simulates sediment dynamics around buildings and their impacts on dune shape, growth and migration. Goldstein and Moore (2016) used GP to develop a simplified 1-D model for coastal foredune height, parameterizing dune growth and erosion by storms. In terms of aeolian sediment transport process-based models, Aeolis (Hoonhout & de Vries, 2016) is a multi-fraction model that simulates spatiotemporal variations in bed surface properties and sediment availability. Based on the work of Durán and Herrmann (2006) and de M. Luna et al. (2011) developed a 2D dune formation model that employs a quantitative description of the turbulent wind field over the terrain with a continuum saltation model

21699011, 2023, 9, Downloaded from https://agupubs.onlinelibrary.wiley.com/doi/10.1029/2023JF007080 by Cochrane Portugal, Wiley Online Library on [06/11/2023]. See the Terms and Conditions (https://onlinelibrary.wiley.com/terms-and-conditions) on Wiley Online Library for rules of use; OA articles are governed by the applicable Creative Commons License

and vegetation growth. Based on the same work, the coastal dune model (CDM; Durán & Moore, 2013) focuses on resolving airflow, sediment transport and vegetation growth.

Models that couple marine and aeolian processes across the beach-dune profile, can integrate a significant level of interactions across scales and can be useful tools to explore complex morphodynamic feedback mechanisms (Cohn et al., 2019) and the role of vegetation and sediment supply in the development of the shape of foredunes (Roelvink & Costas, 2019). Windsurf (Cohn et al., 2019) couples three models which simulate subtidal morphodynamics related to waves and currents (XBeach), subaerial morphodynamics related to wind shear and vegetation (CDM), and multi-fraction aeolian sediment transport that includes the effects of supply limiters (Aeolis). XBeach-Duna (Roelvink & Costas, 2019) couples two process-based (marine and aeolian) models over the beach-dune profile and was tested over multidecadal timescales. Duna comprises a wind flow module, a flow-vegetation interaction module and a sand transport module and accounts for a wide array of supply limiting conditions (armoring, fetch limitation, moisture, slope). For long-term simulations, approaches combining machine learning algorithms with morphodynamic models to reduce computational loads, such as the Long Short-Term Memory model paired with Windsurf (Itzkin et al., 2022), have also been employed. Similarly, simplified semi-empirical models, such as the cross-shore sediment transport (CS) model (Hallin et al., 2019) that solves conceptual morphological models for the coupled evolution of beach-dune systems, have been used over decadal to centennial time scales.

Despite recent advances in morphodynamic modelling of coupled coastal processes, simplified approaches and reduced complexity numerical models are likely the solution for long-term coastal change simulations (Ranasinghe, 2020). A major challenge in using simplified models is assessing whether numerical results accurately emulate real world processes (R. Davidson-Arnott et al., 2018), making rigorous calibration and validation essential. Still, after appropriate calibration and validation, such approaches could help understanding long-term dune morphodynamics, often constrained by contextual limitations related to spatial and temporal scales (Walker et al., 2017).

From the above, it can be deduced that open issues exist in coastal dune morphodynamics and that numerical models can potentially provide valuable information, otherwise difficult or impossible to extract from field measurements. Among the currently open questions and controversies is the influence of dune shape on dune growth and the role of internal and external controlling factors, while the existence of a maximum dune height has been strongly debated. The present study aims to elucidate the influence of dune topography (dune height and stoss slope) and vegetation cover on wind flow, sand transfer and deposition on the dune for different beach and wind incidence conditions. To this aim, a series of idealized numerical experiments are performed using an updated version of the Duna process-based model that includes parameterization of the fetch effect, after calibration and validation against numerical and field data. The idealized experiments include variable dune morphologies (dune heights: 4–26 m and stoss slopes: 0.29–0.5), wind incidence angles (0°–75°), vegetation densities and beach widths. The results are used to identify wind flow and short-term sand accumulation patterns with relation to dune shape over the beach-dune profile and to gain insights on related dune growth/adaptation mechanisms and potential limiting conditions.

2. Methods and Data

2.1. Duna Morphodynamic Model

In the present paper, we employ a standalone version of the 1D Duna model (Roelvink & Costas, 2019), a morphodynamic model that simulates the evolution of dunes as a result of input conditions (e.g., wind, vegetation cover) and of the dynamic interactions and feedbacks between morphology, flow and vegetation. The computational flow in Duna is as follows: (a) calculation of the wind velocity field along the beach-dune topographic profile, (b) reduction of wind velocity in vegetated areas of the dune due to plant-wind interaction, (c) critical shear stress calculation along the profile, accounting for moisture and slope effects for sand transport, (d) definition of instantaneous sediment concentrations in the domain, accounting for additional transport limiting parameters (fetch and armoring), and (e) update of the dune topography (solution of 1D advection and mass balance) and of the vegetation cover.

As Duna model has been thoroughly analyzed in Roelvink and Costas (2019), here we briefly mention the main model parameterizations, focusing on recent improvements and providing formulas that are new or pertinent to the present work (the reader is referred to Roelvink and Costas (2019) for the extended analysis of model parameterizations).

2.1.1. Brief Model Description

The variability of wind velocity along the dune profile is based on the Kroy model (Kroy et al., 2002a, 2002b). The Kroy wind shear stress model involves two constants, α and β, used to tune the model (calibration parameters). Both

21699011, 2023, 9, Downloaded from https://agupubs.onlinelibrary.wiley.com/doi/10.1029/2023JF007080 by Cochrane Portugal, Wiley Online Library on [06/11/2023]. See the Terms and Conditions (https://onlinelibrary.wiley.com/terms-and-conditions) on Wiley Online Library for rules of use; OA articles are governed by the applicable Creative Commons License

constants depend logarithmically on the ratio L/z_0, where L is the characteristic length of the dune (i.e., half of the width at half-height of the Gaussian heap assumed in the analytic solution) and z_0 is the surface roughness length (Kroy et al., 2002a, 2002b; Roelvink & Costas, 2019). Using the analytic expression of Kroy et al. (2002a), the values of α and β can be estimated, based on dune shape (e.g., values range from $\alpha = 5.25$ and $\beta = 0.32$ for $L/z_0 = 4 \cdot 10^3$ to $\alpha = 3.5$ and $\beta = 0.2$ for $L/z_0 = 4 \cdot 10^6$). Given that the Kroy model is applied in Duna to assess the influence solely of topography on the bed shear (the influence of vegetation is accounted for separately, i.e., see Buckley formula in Equation 1), z_0, α, and β can be considered constant throughout portions of the profile with uniform slopes.

The simplified wind model cannot reproduce flow separation at the lee of the dune. To account for that, a condition of no sediment pickup is applied within the zone of the separation bubble (leeslope effect), which is assumed to occupy the zone of the lee (downwind from the crest brink) below an angle equal to the critical slope for flow separation (~14°) and the horizontal (Kroy et al., 2002a).

The interference of vegetation with the flow has been estimated using the simplified formula of Buckley (1987), assuming that the damping of the depth-averaged velocity, induced by a patch of plants with coverage C_V, is (Roelvink & Costas, 2019):

$$\left.\frac{U}{U_0}\right|_V = 1 - k \cdot C_V \tag{1}$$

In the formula, k is a constant dependent on the plant characteristics. According to Buckley (1987), who tested C_V values up to 17%, k is 0.018 for typical small erect or spreading herbaceous plants and reaches 0.046 for small stemless rounded plants.

The critical shear stress velocity for sand motion is calculated by the Bagnold formula (Bagnold, 1936), multiplied by a slope term that accounts for the upslope increase, or downslope decrease, of the shear velocity, compared to a horizontal surface. The model also accounts for the influence of moisture on the threshold for the motion of sand (i.e., by sea level oscillations and swash, e.g., obtained from XBeach in coupled runs), effects that are omitted in the idealized experiments presented, for simplicity and comparability between the results. Transport limitation due to armoring is also included, considering a two-layered structure of the sediment, with the upper layer consisting of sand (transportable by winds) and a much coarser underlying layer (essentially non-transportable by aeolian events), in a similar but significantly more simplified approach to the one of Hoonhout & de Vries (2016). In long-term beach-dune coupled simulations, the armoring effect is frequently removed by "reset" events (e.g., due to swash, extreme wind events, or people) in-between aeolian events (Roelvink & Costas, 2019).

The saturated (or equilibrium) concentration, calculated from the Bagnold sediment transport rate formula, is used to calculate the instantaneous concentration assuming a relaxation timescale for sediment pickup (~1 s) (Hoonhout & de Vries, 2016) and an empirical upper limit of 2 kg/m^2. Sediment fluxes along the grid are determined using a 1-D upwind advection scheme and the mass balance in each grid cell is translated to elevation change (considering the porosity and density of sand). If the slope of the simulated profile exceeds the angle of repose, avalanching occurs, and the sediment is redistributed assuming a post-avalanching slope equal to the angle of repose. Simulated topographic changes in each temporal step are used to update vegetation characteristics (height and density) due to sand burial and potential plant mortality due to excessive erosion (i.e., full exposure of the roots and plant die-off occur for erosion exceeding a critical height ~0.2 m).

2.1.2. New Parameterizations

The sediment transport module is modified in the present application, adding a parameterization of the fetch length influence for sand transport. This is based on the functions proposed by Delgado-Fernandez (2010), reducing the transport calculated by the Bagnold equation by a factor C_{Fetch}:

$$C_{\text{Fetch}} = \begin{cases} \sin\left(\frac{\pi}{2} \cdot \frac{F}{F_C}\right) & F < F_C \\ 1 & F \geq F_C \end{cases} \tag{2}$$

where F_C is the critical fetch length, calculated from the wind velocity magnitude at 10 m from the surface, U_{10}, as follows:

$$F_C = 4.38 \cdot U_{10} - 8.23 \tag{3}$$

21699011, 2023, 9, Downloaded from https://agupubs.onlinelibrary.wiley.com/doi/10.1029/2023JF007080 by Cochrane Portugal, Wiley Online Library on [06/11/2023]. See the Terms and Conditions (https://onlinelibrary.wiley.com/terms-and-conditions) on Wiley Online Library for rules of use; OA articles are governed by the applicable Creative Commons License

To account for the combined influence of topography and fetch under oblique wind incidence, the computational grid is rotated by an angle, θ, equal to the angle between the initial profile and the direction of the wind. Grid rotation was performed assuming "infinite" and uniform topography alongshore and projecting the profile onto the wind direction (Figure S2 in Supporting Information S1). Essentially, this translates to a horizontally stretched profile, with a projected computational grid step of

$$dx' = \frac{dx}{\cos\theta} \tag{4}$$

The projected profile is used throughout the flow and sand transport modules of Duna and morphological changes are transferred to the initial profile at the end of each step (aeolian event).

2.1.3. Model Assumptions and Simplifications

Duna simulates sediment transport by saltation, initiated and sustained by the wind flow (disregarding suspension flows). Topographic forcing and steering effects, near-surface flow deflection and acceleration patterns and local secondary flows that can be important for modeling foredune morphodynamics (Hesp et al., 2015; Walker et al., 2006, 2009) are not included in the 1-D flow model. Also, the assumption of a logarithmic wind velocity profile, used to calculate the shear velocity, may not hold near the foredune crest (Bauer et al., 2022). In the present model applications, we also disregard marine influences (i.e., no armoring or moisture effects) and consider one type of non-flexible dune plant throughout the modeled profile for the idealized experiments.

In terms of boundary conditions, infinite sediment supply is assumed at the upwind boundary (theoretical seaward limit of dry beach) and an open boundary is applied at the landward limit of the computational grid.

2.2. Simulations and Data Sets

As already noted in the introduction, the focus of the work is to assess how internal (dune shape and vegetation cover) and external (beach width, wind angles) factors affect short-term dune morphologic change through idealized simulations. Prior to extracting meaningful information and conclusions from numerical results, their reliability needs to be determined and verified. Thus, a necessary first step in the analysis is to assess the model accuracy and its ability to reproduce dune morphodynamics under different conditions. This is performed in the first set of simulations, implemented for calibration and validation of the flow and sediment transport modules of Duna. These simulations aim to emulate real conditions, using validated modeling results or field measurements from different coastal dune sites. After calibration and validation, a series of idealized experiments are performed, designed to identify the influence of dune shape (height and stoss slope) on wind flow and sand transfer along the dune profile under variable wind incidence (onshore, oblique and highly oblique winds). The sand transfer experiments were performed for different fetch (limited and non-limited) conditions and vegetation densities (low to very high). Below, we outline the characteristics of each experiment and the data used.

2.2.1. Calibration/Validation Data and Conditions

Four calibration/validation experiments were implemented, two for the wind flow module and two for the sediment transport modules of Duna, which are hereon referred to as Wind1, Wind2, Morpho1, and Morpho2, respectively. The conditions and data sets used in each simulation are detailed below and summarized in Table 1.

Simulation Wind1 (Table 1) uses the CFD model results of Hesp and Smyth (2016), to calibrate and validate the Kroy model (constants α and β), comparing the two model results for variable wind incidence angles. The CFD numerical experiments of Hesp and Smyth (2016) were conducted over a foredune stretch on the Greenwich Dunes of the Prince Edward Islands (Canada), with a crest at 8–9 m above mean water level and a steep stoss slope (20°–25°). The CFD simulations were conducted for 2D topographic profiles (horizontal grid step of 0.25 m, variable vertical step from 0.1 to 1.36 m from surface to upper boundary) over the foredune, ranging from 0° (onshore) to 70° (obliquely alongshore) winds and varying wind speeds. Here, we used results from the set of experiments considering wind storm conditions (wind speed of 10.57 m/s at 1 m from the bed; Table 1) corresponding to, and partially validated by, field measurements during a gale event at the site (Hesp et al., 2009, 2013).

In simulation Wind2 (Table 1), the wind flow calibration was tested against the wind measurements of Schwarz et al. (2021), conducted in a steep (21.8°) and high (20 m) dune near Egmond aan Zee, in the Netherlands, over

21699011, 2023, 9, Downloaded from https://agupubs.onlinelibrary.wiley.com/doi/10.1029/2023JF007080 by Cochrane Portugal, Wiley Online Library on [06/11/2023]. See the Terms and Conditions (https://onlinelibrary.wiley.com/terms-and-conditions) on Wiley Online Library for rules of use; OA articles are governed by the applicable Creative Commons License

Table 1
Data for Calibration/Validation Experiments

Simulation	Wind flow		Morphodynamics	
Name	Wind1	Wind2	Morpho1	Morpho2
Type	CFD model	Field data	Field data	Field data
Reference	Hesp and Smyth (2016)	Schwarz et al. (2021)	Brodie et al. (2019)	Costas et al. (2020)
Site	Prince Edward Island, Canada	Egmond aan Zee, the Netherlands	FRF, Northern Outer Banks, USA	Praia de Faro, Ria Formosa, Portugal
Dune height	8.75 m	20 m	7.35 m	7 m
Stoss slope	20°	21.8°	30°	7°
Duration	Stable model solution	5 weeks (October 2017)	35 days (11 April −16 May 2016)	1 year (April 2017 –March 2018)
Input topo	RTK-DGPS DEM	RTK-GPS profile, 31 October 2017	LiDAR April 2016, TDS Catalog (2022)	UAV data, April 2017
Input wind	U1 = 10.57 m/s	U1 from U10; IJmuiden station	U10 from U18.9; CS05, TDS Catalog (2022)	U10; Faro Airport station (Costas et al., 2020)
C_V	n.a.	n.a.	0.4–0.75	0.2–0.7
Buckley k	n.a.	n.a.	0.55	Stoss: 0.2 Crest-lee: 0.45
Tidal ampl.	–	–	1 m	1.5 m
Wave runup	–	–	0 m	Calm: 0.75 m Storm: 4 m
Marine storms	–	–	–	Post-Emma UAV beach profile
Validation data	Gridded (dx = 0.25 m) U1; W angles 10°–70°	UAs: U1 at toe, slope & crest (at 3, 11 and 18 m)	LiDAR May 2016, TDS Catalog (2022)	UAV data, March 2018

Note. C_V: dune vegetation density, given as value range from toe to crest; Buckley k: constant in Equation 1; CFD: Computational Fluid Dynamics; UA: Ultrasonic Anemometer; U1, U10, and U18.9: wind speed at 1, 10, and 18.9 m from surface; DEM: Digital Elevation Model; FRF: Field Research Facility; UAV: Unmanned Aerial Vehicle.

a period of 5 weeks in October 2017. During the experiment, wind direction and magnitude were recorded using 3D ultrasonic anemometers (UAs) in 3 locations across the foredune: at the dune toe (UA1, ∼3 m), at the stoss slope (UA2, ∼11 m) and at the dune crest (UA3, ∼18 m). Schwarz et al. (2021) used data from a nearby offshore station (IJmuiden) as reference for undisturbed wind conditions. This data set was used as forcing wind time series for Wind2 after transforming the input winds (at 10 m from surface) to the measurement elevation of the UAs (∼1 m from ground) using the law-of-the-wall.

Regarding morphodynamic simulations (results in Section 3.1.2), runs Morpho1 and Morpho2 were performed using field data collected during accretional events in two coastal dune areas (using calibrated Kroy constants from Wind1&2). Morpho1 (Table 1) focuses on the dunes at the Field Research Facility (FRF), in the Northern Outer Banks barrier islands of North Carolina (USA). Field measurements were conducted on a sandy, dune-backed, microtidal, intermediate beach, oriented at around −18° to north, with fine to coarse sand and average foreshore slope of 1:12 (Brodie et al., 2019). Accretive dynamics for FRF were simulated for the north part of the dune (y = 895 m) during a period of Nor'easters between 11 April and 16 May 2016 (Brodie et al., 2019). This specific event was selected due to its low impact of marine conditions on the dune. Therefore, only the influence of tidal levels (amplitude of 1 m) on the dry beach width was considered in the simulation. Wind data (measured at an elevation of 18.9 m and transferred to 10 m using the law-of-the-wall) and LiDAR data were obtained from the TDS Catalog (2022), while dune vegetation density (C_V) was estimated to range from 0.4 at the dune toe to 0.75 at the crest, from the data presented in Brodie et al. (2019).

Morpho2 (Table 1) focuses on Praia de Faro, in the westmost barrier of the Ria Formosa (south Portugal), a mesotidal, intermediate, coarse sandy beach, oriented at around 127° to north (Costas et al., 2020), and with fore-

21699011, 2023, 9, Downloaded from https://agupubs.onlinelibrary.wiley.com/doi/10.1029/2023JF007080 by Cochrane Portugal, Wiley Online Library on [06/11/2023]. See the Terms and Conditions (https://onlinelibrary.wiley.com/terms-and-conditions) on Wiley Online Library for rules of use; OA articles are governed by the applicable Creative Commons License

shore slopes of 1:6–1:15. The simulated period is April 2017–March 2018, during which two storms impacted the area (Costas et al., 2020). The first one (Ana storm; 10 December 2017) coincided with neap tides and low water levels and was essentially a wind event, with westerlies exceeding 9 m/s (10 min average velocities) for almost 12 hr. The second one (Emma storm, 28 February–3 March 2018) was an intense wave event, coinciding with spring tides and considerable storm surge levels (Ferreira et al., 2019). Combined to the heavy rainfall that occurred, this event likely caused limited aeolian transport, despite the intense westerly winds (average velocities over 9 m/s for circa 74 hr), but it did induce berm erosion and strong flattening of the shore (Kombiadou et al., 2021). To account for the morphological impact of the storm to sand availability, the reduction of the beach slope after the incidence of Emma was hard-coded to the simulations. Reduction of the dry beach due to tides (amplitude of 1.5 m) and wave runup (height of 4 m for storm—i.e., during Emma—and 0.75 m for non-storm conditions) was also considered. Topographic profiles (extracted from DEM data) and wind data, collected by a nearby station and converted to local winds (Costas et al., 2020), were used as initial and forcing data sets.

2.2.2. Idealized Experiments Data and Conditions

To assess the influence of dune morphological characteristics on wind flow and sediment accumulation patterns over the dune, we designed a set of idealized experiments, assuming a simplified dune profile with varying stoss slopes (1/3.5, 1/3, 1/2.5, and 1/2) and dune heights (4, 6, 10, 14, 18, 22, and 26 m). The dry beach has stable slope (0.0125) and variable widths to simulate distinct sediment delivery to the dune (fetch-limited and non-limited conditions). Results are analyzed by grouping wind incidence in three directional bins: onshore ($\theta \leq 15°$), oblique ($15° < \theta \leq 45°$) and highly oblique ($45° < \theta \leq 75°$) winds.

The wind flow experiments (results in Section 3.2.1) are performed with no morphologic changes to the dune profile and using the input wind velocity time series from the Wind2 experiment (Schwarz et al., 2021). For the sand transport experiments, a synthetic wind velocity time series is compiled, using velocity magnitudes from the Wind2 input data set (150 hr, with wind speeds between 5.40 and 22.72 m/s and average of 12.92 ± 2.34 m/s), repeated for changing wind directions, so that the same wind magnitudes and frequencies are considered for each wind directional bin. The critical fetch length (F_C), corresponding to the velocity magnitude of the synthetic time series, ranges between 15.4 and 91 m, with an average of 48.4 ± 10.2 m. To ensure that results are comparable in terms of morphologic change between the three wind directional bins, dune morphology and vegetation are initialized at the beginning of each bin.

In terms of vegetation density, linearly varying values were assumed between the lower stoss (1 m from the toe) and the crest and uniform values thereon landwards. Different conditions of vegetation coverage were run, including low, high and very high vegetation densities (hereafter LD, HD, VHD, respectively). The density ranges, set for these runs, are LD = [0.2 0.6], HD = [0.5 0.7], and VHD = [0.8 1.0], while the Buckley constant used was $k = 0.7$. The impact of dune morphology to sand transfer under different beach conditions and wind incidence angles was assessed by the non-limited (NL; results in Section 3.2.2) and fetch-limited (FL; results in Section 3.2.3) experiments, considering beach widths of 200 and 50 m, respectively. The characteristics and input data of the idealized experiments are summarized in Table 2.

3. Results

3.1. Calibration/Validation Simulations

3.1.1. Wind Flow

The comparison of simulated wind velocities along the dune profile from Wind1 against the CFD model results of Hesp and Smyth (2016) (details in Table 1) is given in Figure 1 as values normalized to the incident wind speed and for wind directions varying from onshore (0°) to highly oblique (70°) winds. The results were obtained for Kroy constants of $\alpha = 3$ and $\beta = 0.2$ over the foredune slope and are given for simulations with and without rotation of the computational grid. The difference between the two runs (rotated and non-rotated; R and NR, respectively) is plotted in the bottom panels of each wind angle experiment in Figure 1. The same panels show the variability of absolute error between each run and the CFD model up to the crest brink and goodness-of-fit indicator (nondimensional velocity root mean square error (RMSE) and Brier Skill Score (BSS); Brier (1950)) values.

Results show good agreement of the Duna rotated grid simulations with CFD along the windward side of the dune, with modeled velocities capturing the extension and intensity of the wind reduction in the dune toe and

21699011, 2023, 9, Downloaded from https://agupubs.onlinelibrary.wiley.com/doi/10.1029/2023JF007080 by Cochrane Portugal, Wiley Online Library on [06/11/2023]. See the Terms and Conditions (https://onlinelibrary.wiley.com/terms-and-conditions) on Wiley Online Library for rules of use; OA articles are governed by the applicable Creative Commons License

Table 2
Data for Idealized Experiments

Parameters	Wind flow experiment	Sediment transport experiments	
		NL	FL
SS	All	All	All
DH	All	All	All
beach width	90 m	200 m	50 m
C_V	–	LD, HD, VHD	HD, LD
Input wind	Same as Wind2	Synthetic: initial 150 hr wind speed from Wind2, repeated for onshore, oblique and highly oblique incidence angles	

Note. NL: non-limited conditions; FL: fetch-limited conditions; SS: stoss slope (all: 1/3.5, 1/3, 1/2.5, and 1/2); DH: dune height (all: 4, 6, 10, 14, 18, 22, and 26 m); LD: low density, $C_V = [0.2\ 0.6]$, HD: high density, $C_V = [0.5\ 0.7]$, and VHD: very high density, $C_V = [0.8\ 1.0]$.

the gradual increase over the stoss slope up to the dune crest, fairly well, for all wind directions. In the leeside of the dune, the velocity drop directly downwind from the crest is accurately captured by the model; however, there is high and consistent underestimation of the flow attenuation in the remainder of the dune lee. Given that the Kroy model is assessing the influence of topography, and namely the slope of the landform, on flow deformation and that the lee slope of the dune tested is lower than the stoss slope, it is expected that the model does not simulate a higher flow damping in the downwind than the upwind side of the dune. It is noted that the impacts of the inability of the simplified Kroy model to reproduce the flow separation at the lee of the dune to sand transport are amended in the morphodynamic module of Duna through the introduction of the leeslope effect (mentioned in Section 2.2.1).

Comparing the two versions of the model (R and NR, shown in the lower panels of Figure 1), the two sets of results practically overlap for near-onshore winds (≤30°), with little difference in accuracy against the CFD data. It is noted that the peak reduction of the velocity at the toe is slightly overestimated by the model for near-onshore winds (peak absolute error of 0.19–0.24). As the projected dune stoss slope, used in the R Duna runs, varies with the cosine of the wind incidence angle, it follows that the difference between projected and non-projected dune topography remains low for low incidence angles (e.g., slope decrease of 13.4% in projected stoss for 30°) and increases with wind obliquity for higher angles (e.g., slope decrease in projected stoss from 23.4% for 40° to 65.8% for 70°). For higher wind incidence angles (>30°) the NR grid simulation consistently underestimates wind speed, while the Duna accuracy improves notably in the R grid simulations. The RMSE of R versus NR simulation ranges from 0.047 versus 0.058 ($\theta = 40°$) to 0.036 versus 0.048 ($\theta = 70°$), while in terms of BSS values range between 0.95 versus 0.92 ($\theta = 40°$) and 0.78 versus 0.58 ($\theta = 70°$). It follows that the introduction of grid rotation to Duna improved the approximation in terms of wind flow and topography interaction.

The results of simulation Wind2 for the field wind measurements of Schwarz et al. (2021) (details in Table 1) are given in Figure 2, considering the calibrated values for the Kroy constants ($\alpha = 3$ and $\beta = 0.2$) from Wind1. Wind velocities measured by the 3 UAs in the field are compared to simulated values at the same elevation along the foredune profile for onshore to highly oblique wind incidence (0°–75°): UA1 at the dune toe (~3 m; Figure 2a), UA2 at the stoss slope (~11 m; Figure 2b) and UA3 at the dune crest (~18 m; Figure 2c). The agreement between simulated and measured velocities is good in all 3 measurement points, with RMSEs of 1.01, 1.33, and 2.03 m/s (values normalized to input wind speed: 0.11, 0.14, 0.22) at UA1, UA2, and UA3, respectively. There is a tendency for the overestimation of velocity by the model, which becomes more pronounced with wind obliquity, especially at the stoss and the crest (Figure 2). Due to the simplified 1D modeling approach used, influences of microtopography and alongshore nonuniformity of the foredune ridge on the flow (i.e., topographic steering) cannot be reproduced. Overall, model performance is considered good, confirming that the simplified model can reproduce the major trends in wind flux along the profile fairly accurately, even in challenging cases of very high dunes.

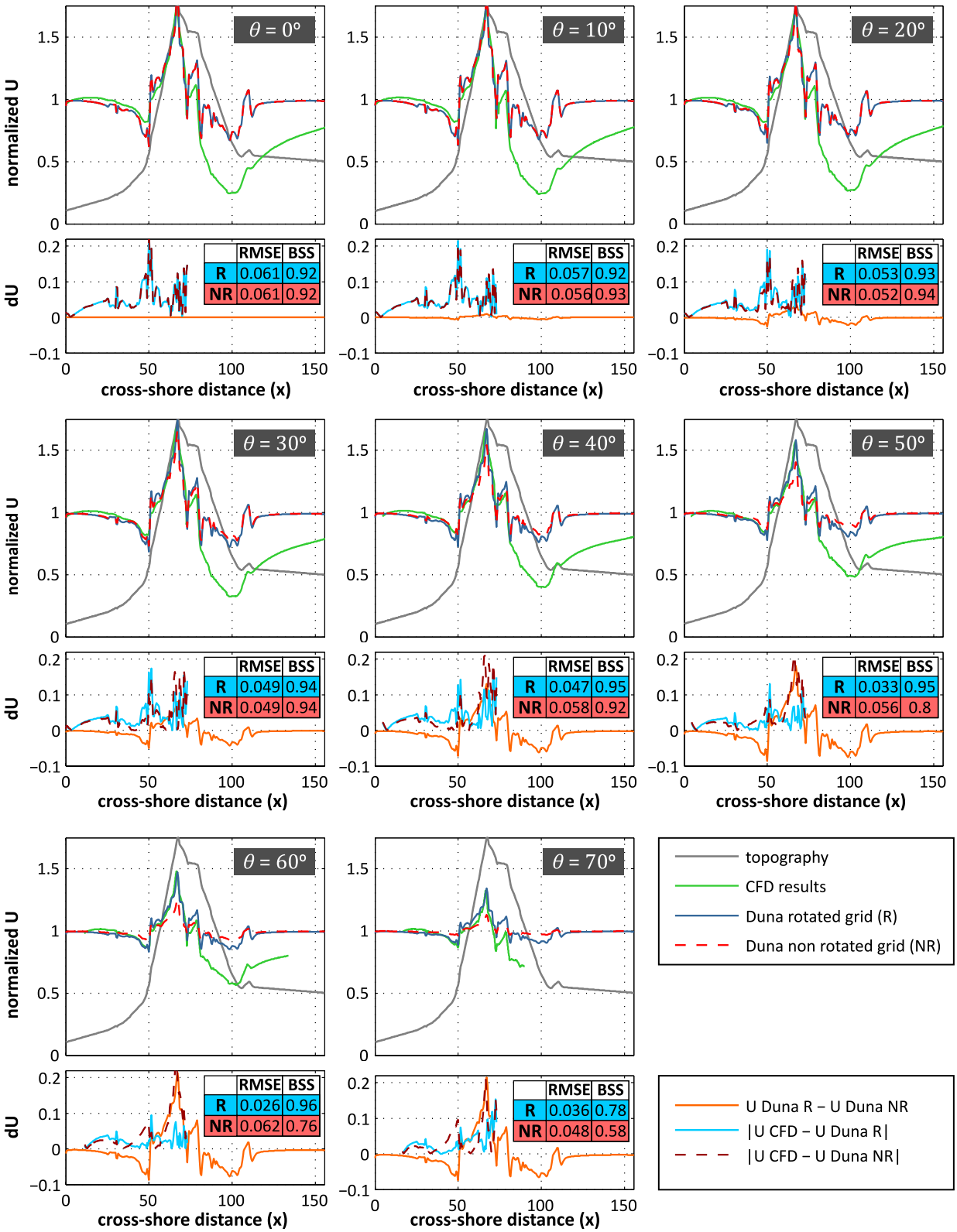

Figure 1. Results of Wind1, showing the comparison of computational fluid dynamics (CFD) model results from Hesp and Smyth (2016) with Duna model runs (wind incidence $\theta = 0°$–$\theta = 70°$) with and without grid rotation (green solid, blue solid and red dashed lines, respectively); the gray curve provides the dune morphology (vertical scale is compressed by 1.75/8). The lower panels show the difference in simulated velocity between Duna rotated (R) and non-rotated (NR) runs (orange line) and the absolute error of R and NR Duna runs along the windward dune side, with reference to the CFD results (solid light blue and dashed dark red lines, respectively); nondimensional velocity root mean square error and Brier Skill Score values are given in each plot. All velocities are normalized to the offshore velocity speed.

21699011, 2023, 9, Downloaded from https://agupubs.onlinelibrary.wiley.com/doi/10.1029/2023JF007080 by Cochrane Portugal, Wiley Online Library on [06/11/2023]. See the Terms and Conditions (https://onlinelibrary.wiley.com/terms-and-conditions) on Wiley Online Library for rules of use; OA articles are governed by the applicable Creative Commons License

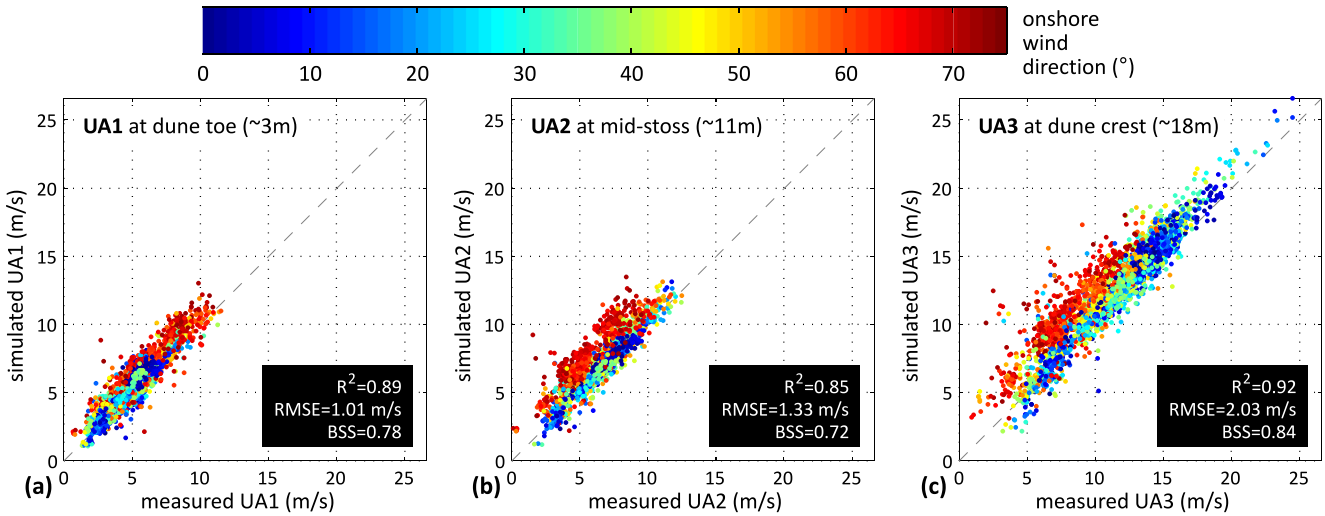

Figure 2. Results of Wind2, showing the comparison of measured (*x*-axes; data from Schwarz et al. (2021)) and simulated (*y*-axes) wind speed (m/s) at the dune toe (UA1, in (a)), mid-stoss (UA2, in (b) and crest (UA3, in (c); colors denote onshore wind direction (reference to color bar), perfect agreement is denoted by a gray-dashed line and goodness of fit indicators are provided in each plot.

3.1.2. Morphodynamics

Following the calibration and validation of wind flow in Duna, we proceed with the calibration and validation of sand transport during accretional events in two coastal dune areas (using the calibrated wind flow constants; see details on experiments Morpho1 and Morpho2 in Table 1). Comparison of measured and simulated morphological changes for experiment Morpho1, assuming a Buckley constant (k in Equation 1) of 0.55, are given in Figure 3. The simulation underestimates sand transfer to the dune by around 7%, with a difference in total volume change of -0.12 m^3/m between simulation and measurement. The overall RMSE in the simulated profile elevation is 0.12 m, with a small overestimation of accumulation at the dune toe (up to $x = -55$ m; RMSE = 0.1 m) and underestimation at the mid-upper stoss (between $x = -55$ to -52 m; RMSE = 0.16 m). Peak accumulation at the dune crest is accurately reproduced (0.16 vs. 0.17 m), with low underestimation along the lee (RMSE of 0.07 m; total volume error of -0.35 m^3/m). The simulated and measured landward extension of sand transfer in the profile overlap ($x = -45$ m).

The results of the 1-year Morpho2 (see Table 1 and Section 2.2.1 for input data) simulation are given in Figure 4, where the morphological impact of the Emma storm to the beach (hard-coded to the simulations) is also shown. The Buckley constant (k in Equation 1) was set to 0.2 in the stoss and 0.45 from the crest on landwards. Overall, the model captures the total volume change ($dV_{sim} - dV_{obs} = -0.37$ m^3/m), the areas of sediment accumulation and the range of the vertical accretion (RMSE: 0.13 m). At the same time, it does tend to uniformize the profile, flattening out small-scale humps, likely due to the non-variable vegetation properties (density and Buckley constant) set throughout the entire morphological parts of the foredune. In the crest, where three pronounced peaks are found, the total accumulated volume is simulated at 2.24 m^3/m, whereas the corresponding measured value is 2 m^3/m. This confirms that accumulated sand is well simulated, while the main disagreement is in microtopographic variability, which the model is unable to reproduce because it assumes uniform values, disregarding the patchy organization of the vegetation in the field. Along the leeward face of the dune (Figure 4), the accumulation is well reproduced, with higher accumulation simulated directly downwind from the crest brink. The RMSE and the total volume difference between modeled and measured accumulation over the lee are 0.18 m and 0.28 m^3/m, respectively. It follows that the error in the simulation over this zone is low and mainly due to the higher sedimentation directly after the crest brink, while the landward extent and total volume of accumulation are well represented. It is noted that a test simulation to assess whether assigning spatially varying vegetation parameters would allow to maintain microtopographic features was also run. In this test, very high vegetation density (~0.8) was set in the vicinity of the local peaks. The simulated profile (not shown) maintained the initial microtopographic features on and around the peaks and reproduced vertical growth in these zones. As the scope of the work is to assess the overall model performance, the latter is considered an over-tuned calibration set and, thus, was not adopted.

21699011, 2023, 9, Downloaded from https://agupubs.onlinelibrary.wiley.com/doi/10.1029/2023JF007080 by Cochrane Portugal, Wiley Online Library on [06/11/2023]. See the Terms and Conditions (https://onlinelibrary.wiley.com/terms-and-conditions) on Wiley Online Library for rules of use; OA articles are governed by the applicable Creative Commons License

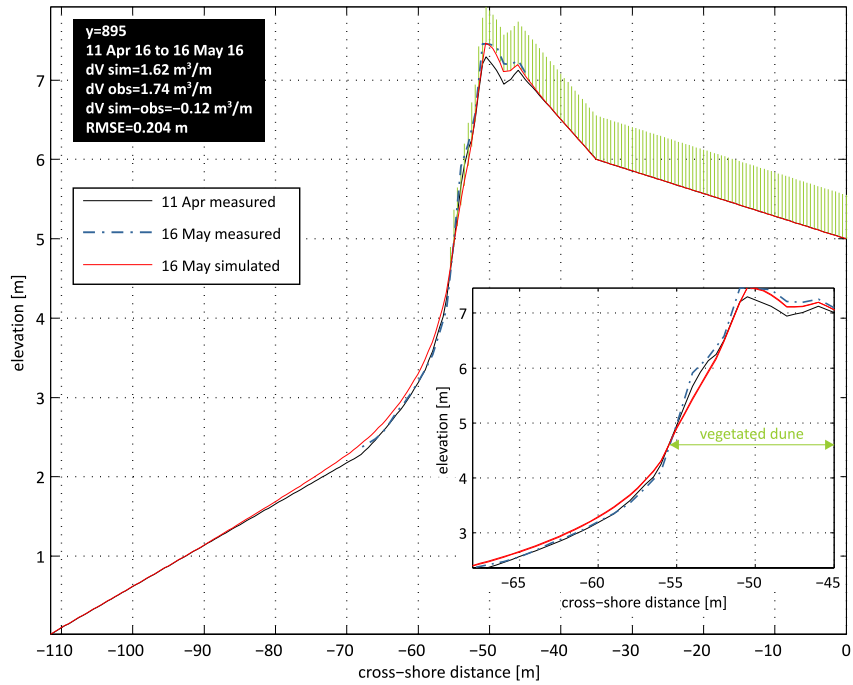

Figure 3. Results of Morpho1, showing the comparison of measured (LiDAR; blue dash-dot line) and simulated (red) dune profiles for the north Field Research Facility dune (y = 895 m in Brodie et al. (2019)) for 16th May 2016. The initial profile (11th April 2016) is given in black, while the green vertical lines indicate vegetation height in the profile at the end of the simulation. The inset plot provides a zoom on the area of the measured profile stretch, while goodness-of-fit indicators are mentioned in the black box (dV is total accreted volume and "sim" and "obs" denote simulation and observation, respectively).

3.2. Idealized Numerical Experiments

The idealized numerical experiments are divided into wind flow and sediment transport simulations, investigating the influence of dune shape parameters on flow deceleration and acceleration patterns (in Section 3.2.1) and on sand accumulation along the dune profile, respectively. Sediment transport experiments initially focus on the influence of beach width on sand transfer in the domain (NL conditions in Section 3.2.2 and FL conditions in Section 3.2.3, assuming HD over the dune), while the impacts of dune vegetation density (LD, HD, and VHD runs) and the sensitivity of the parameterization used to describe the interaction of dune plants with sand fluxes and the impacts on sediment transport patterns are subsequently analyzed (in Section 3.2.4). Sediment transport modeling results are analyzed by splitting the domain into zones (beach to toe, stoss slope, crest and lee), separated at the toe and the windward crest brink. Due to differences in sand transfer toward the lee between experiments, the zones of crest and lee are joined in the analysis, for consistency. Regarding wind incidence, we separate winds into onshore ($\theta \leq 15°$), oblique ($15° < \theta \leq 45°$) and highly oblique ($45° < \theta \leq 75°$) throughout the analysis. Higher angles, corresponding to near-parallel winds, were also tested but were excluded from the present analysis as their impact to the flow is minimal (Walker et al., 2017). Details on the inputs and conditions of each simulation set are given in Table 2.

It is noted that the new parameterization of the fetch effect in Duna and its ability to reproduce the influence of varying fetch lengths on sand transport was verified by testing the impact of beach widths varying from 20 to 120 m (step of 20 m) on a single dune morphology (height of 8 m, slope of 0.4, density HD). The results of this simulation are provided as Supporting Information S1 (Text S1 and Figure S1).

3.2.1. Wind Flow Experiments

The results of the wind flow experiments for the different dune morphologies (combinations of stoss slope and dune height) are shown in Figure 5 as nondimensional velocities (normalized with the input wind velocity magnitude). The panels in the plot correspond to the combination of wind direction (shown in rows; from top to bottom: onshore, oblique and highly oblique) and location in the domain (shown in columns; from left to right: the toe,

21699011, 2023, 9, Downloaded from https://agupubs.onlinelibrary.wiley.com/doi/10.1029/2023JF007080 by Cochrane Portugal, Wiley Online Library on [06/11/2023]. See the Terms and Conditions (https://onlinelibrary.wiley.com/terms-and-conditions) on Wiley Online Library for rules of use; OA articles are governed by the applicable Creative Commons License

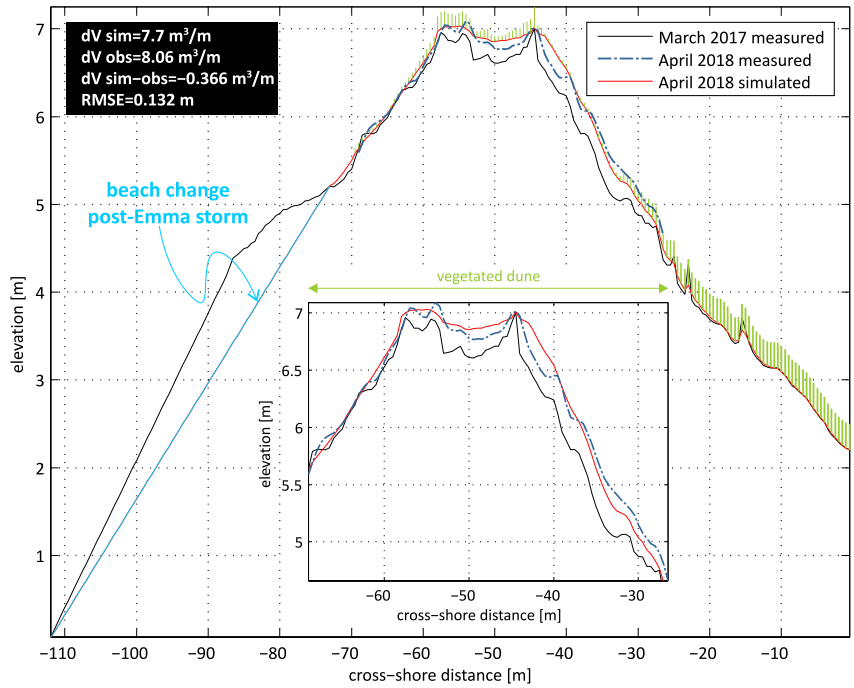

Figure 4. Results of Morpho2, showing the comparison of measured (blue dash-dot line) and simulated (red) dune profiles for Praia de Faro for March 2018. The initial profile (April 2017) is given in black, and the post-Emma storm flattening of the profile included in the simulation is given in light blue, while the green vertical lines indicate vegetation height in the profile at the end of the simulation. The inset plot provides a zoom on the area of the measured profile stretch, while goodness-of-fit indicators are mentioned in the black box (dV is total accreted volume and "sim" and "obs" denote simulation and observation, respectively).

the mid-stoss and the crest). As expected, the interference of the dune topography with the flow is stronger when the dune is higher and/or steeper. Nondimensional velocities at the dune toe (Figures 5a, 5d, and 5g) are below 1 (flow attenuation) and decrease (stronger attenuation) with increasing dune heights and stoss slopes. The opposite trend is observed in the variability at the stoss (Figures 5b, 5e and 5h), with values exceeding 1 (flow acceleration) that increase (stronger acceleration) with height and slope. The same variability in flow speedup is found at the crest (Figures 5c, 5f, and 5i), but with higher values. For increasing wind incidence angles (e.g., at the crest: Figures 5c, 5f, and 5i), the model predicts a decreasing influence of topography on the flow and homogenization of the variability across the profile (normalized velocities closer to 1).

Analyzing the results further, flow stagnation at the toe ranges between 0.47 and 0.75 for onshore winds (Figure 5a). A change in the variability with dune height is noted at the toe as the winds shift from onshore to highly oblique winds (Figures 5a, 5d, and 5g). Flow damping shows low variability with stoss slope for onshore winds (overlapping points for the same dune height), whereas for highly oblique winds the values diverge more between stoss slopes with increasing dune height (e.g., in Figure 5g, variability with slope: 0.87–0.9 for 4-m high dunes, vs. 0.6–0.75 for 26-m high dunes). This means that for onshore winds the impact of stoss steepness is low and, as wind incidence angles increase, slopes gradually become more important. Even though the relative balance between the dune height and slope at the toe varies with wind incidence, nondimensional velocities increase (less attenuation) with wind incidence angle in all morphologies (height-slope combination).

Onshore wind acceleration over the dune stoss is between 1.1 and 1.3 (Figure 5b), while at the crest the values range from 1.3 to 1.8 (Figure 5c), with both areas showing higher variability with stoss slope than the toe (Figure 5a). The acceleration is reduced for higher wind incidence angles at both the stoss and the crest. Still, the model predicts a strong wind speed-up at the crest, even for highly oblique winds, ranging from 1.15 to 1.42 (Figure 5i), while the related values along the stoss are around 1.1 (Figure 5h).

Overall, the variability of wind velocity is largely logarithmic with dune height and linear with stoss slope (reduction at the toe and increase at the stoss and the crest), suggesting that changes to the flow are expected to be

21699011, 2023, 9, Downloaded from https://agupubs.onlinelibrary.wiley.com/doi/10.1029/2023JF007080 by Cochrane Portugal, Wiley Online Library on [06/11/2023]. See the Terms and Conditions (https://onlinelibrary.wiley.com/terms-and-conditions) on Wiley Online Library for rules of use; OA articles are governed by the applicable Creative Commons License

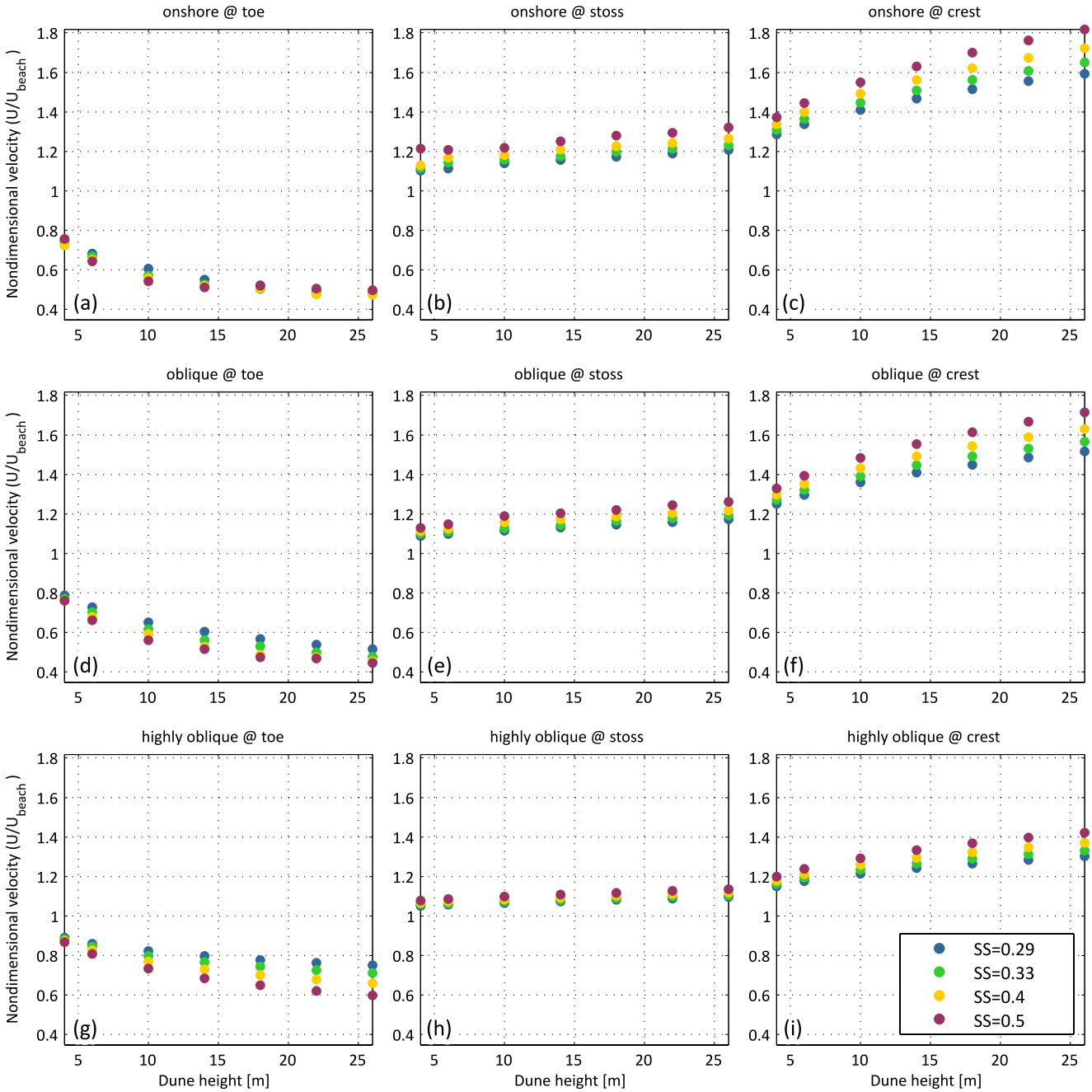

Figure 5. Variability of wind speed (y axis, nondimensionalized with undisturbed wind speed at the beach) with dune height (x axis), at the dune toe (left, (a), (d), and (g)), mid-stoss (center, (b), (e), and (h)) and crest (right, (c), (f), and (i)) for onshore (top, (a)–(c); 0°–15°), oblique (middle, (d)–(f); 15°–45°) and highly oblique (bottom, (g)–(i); 45°–75°) winds and for the 4 stoss slopes (SS; legend) tested; y-axis limits and scale are maintained for all experiments.

negligible after a certain dune height, while changes due to slope increase can still be important. However, considering that the highest slope tested is close to the angle of repose for sands, this linear increase also has a ceiling value and cannot be infinite in natural dune systems. The variability of the flow with dune height and stoss slope can be described by an equation of the form:

$$X = a \cdot \ln(\mathrm{DH}) + b \cdot \mathrm{SS} + c \tag{5}$$

where DH denotes dune height and SS is stoss slope. Here X denotes the normalized velocity, while the values of coefficients a, b, and c are given in Table 3.

21699011, 2023, 9, Downloaded from https://agupubs.onlinelibrary.wiley.com/doi/10.1029/2023JF007080 by Cochrane Portugal, Wiley Online Library on [06/11/2023]. See the Terms and Conditions (https://onlinelibrary.wiley.com/terms-and-conditions) on Wiley Online Library for rules of use; OA articles are governed by the applicable Creative Commons License

21699011, 2023, 9, Downloaded from https://agupubs.onlinelibrary.wiley.com/doi/10.1029/2023JF007080 by Cochrane Portugal, Wiley Online Library on [06/11/2023]. See the Terms and Conditions (https://onlinelibrary.wiley.com/terms-and-conditions) on Wiley Online Library for rules of use; OA articles are governed by the applicable Creative Commons License

Table 3
Values of Coefficients a, b, c and Correlation of the Fit (R^2) to Equation 5 in Each Wind Bin for All Experiments: Flow Experiments (Where X Represents Normalized Velocity) and Non-Limited (NL) and Fetch-Limited (FL) Transport Experiments (Where X Represents Sand Volume, in m^3/m; Results Correspond to HD Density Values)

		Onshore				Oblique				Highly oblique			
Exp.	Area	*a*	*b*	*c*	R^2	*a*	*b*	*c*	R^2	*a*	*b*	*c*	R^2
Flow	Toe	−0.14	−0.06	0.93	0.94	−0.16	−0.32	1.10	0.98	−0.11	−0.47	1.20	0.95
	Stoss	0.06	0.47	0.87	0.96	0.05	0.33	0.90	0.96	0.03	0.16	0.96	0.97
	Crest	0.20	0.75	0.75	0.98	0.17	0.66	0.79	0.98	0.10	0.41	0.87	0.98
NL	Toe	7.70	15.85	−4.84	0.99	6.39	15.11	−4.50	0.99	2.90	10.20	−2.72	0.99
	Stoss	−7.47	−27.43	28.88	0.91	−5.84	−24.49	24.97	0.91	−2.30	−14.74	14.93	0.91
	Dune	−7.43	−15.73	32.15	0.99	−6.17	−15.31	28.29	0.99	−2.78	−10.87	16.69	0.99
FL	Toe	1.65	9.32	−1.37	0.96	1.63	9.94	−1.49	0.97	1.13	8.55	−0.31	0.98
	Stoss	−6.59	−25.07	24.98	0.91	−5.19	−23.24	22.65	0.90	−2.17	−14.56	14.72	0.89
	Dune	−5.54	−13.41	25.23	0.99	−5.09	−14.03	24.67	0.99	−2.60	−10.55	16.27	0.99

3.2.2. Influence of Dune Morphology on Sediment Accumulation for Non-Limited Conditions

To assess the impact of dune shape (all combinations of dune height and stoss slope) on sand transport under non-limited (NL) conditions, the beach width was set to 200 m (see Table 2 for data). Results of total volume changes for the High Density (HD) case are given in Figure 6. The plot is organized in multiple panels, with the columns showing different areas of the domain: changes to the beach and toe (area windwards from the toe) are shown in the left column panels (Figures 6a, 6d, and 6g), changes over the stoss slope are given in the middle column panels (Figures 6b, 6e, and 6h) and changes within the entire dune (domain landwards from the dune toe) are shown in the right column panels (Figures 6c, 6f, and 6i). As for the case of the wind experiments, the rows in the plot show increasing wind incidence angles: the first row shows onshore winds (Figures 6a–6c), the second row presents oblique winds (Figures 6d–6f) and the third row presents highly oblique winds (Figures 6g–6i).

High accumulation at the toe is noted under onshore wind incidence (Figure 6a), ranging between 10.5 and 27.5 m^3/m and increasing logarithmically with dune height and linearly with stoss slope. At the stoss, accumulation under onshore winds (Figure 6b) decreases with both slope and height, with a shift from accretive to erosive conditions around the dune heights of 10 m (for slope of 0.5) to 18 m (for slope of 0.29). The two lowest dune heights tested show low variability with slope over the stoss, likely because of the small difference in height between them. Given that the experiment corresponds to NL conditions, the total accumulation in the domain is stable for each wind bin (28, 24.3, and 14 m^3/m, for onshore, oblique and highly oblique winds, respectively). It follows that the accumulation over the dune shows the opposite variability to the one at the toe, as it is equal to the total accumulation in the domain (stable for NL per wind direction bin) minus the accumulation at the toe. For onshore winds, the sand deposited onto the dune (decreasing with both dune height and stoss slope; Figure 6c) ranges from 17 m^3/m (lowest, mildest dune) to 1.7 m^3/m (highest, steepest dune).

Largely the same variability with dune size parameters as the one described for onshore winds is noted for higher wind angles in each of the three areas, with a reduction, however, in sand volumes and variability, especially for highly oblique winds. At the dune toe the accumulated sand ranges between 9.2 (lowest, mildest dune) and 23.5 m^3/m (lowest, mildest dune) for oblique winds (Figure 6d) and between 4.7 and 12 m^3/m for highly oblique winds (Figure 6g). For the dune, sand accumulation varies between 14.5 and 1.7 m^3/m for oblique winds (Figure 6f) and 9.2 to 2.5 m^3/m for highly oblique winds (Figure 6i). Over the stoss, the shift to erosion takes place in higher/steeper dunes as wind angles increase. For oblique winds (Figure 6e), the shift takes place between heights of 12 m (for slope of 0.5) and 23 m (for slope of 0.29). For highly oblique winds and over the range of dune heights tested, only the steepest slope (0.5) appears erosive for heights above 22 m (Figure 6h). This is due to the relaxation of the impact of topography on wind flow for higher wind incidence angles (Figures 1 and 5).

Overall, the results show that increasing wind incidence angles are associated with the reduction of accumulated volumes and a decrease in the variability of values within each area. Considering the entire range tested, the

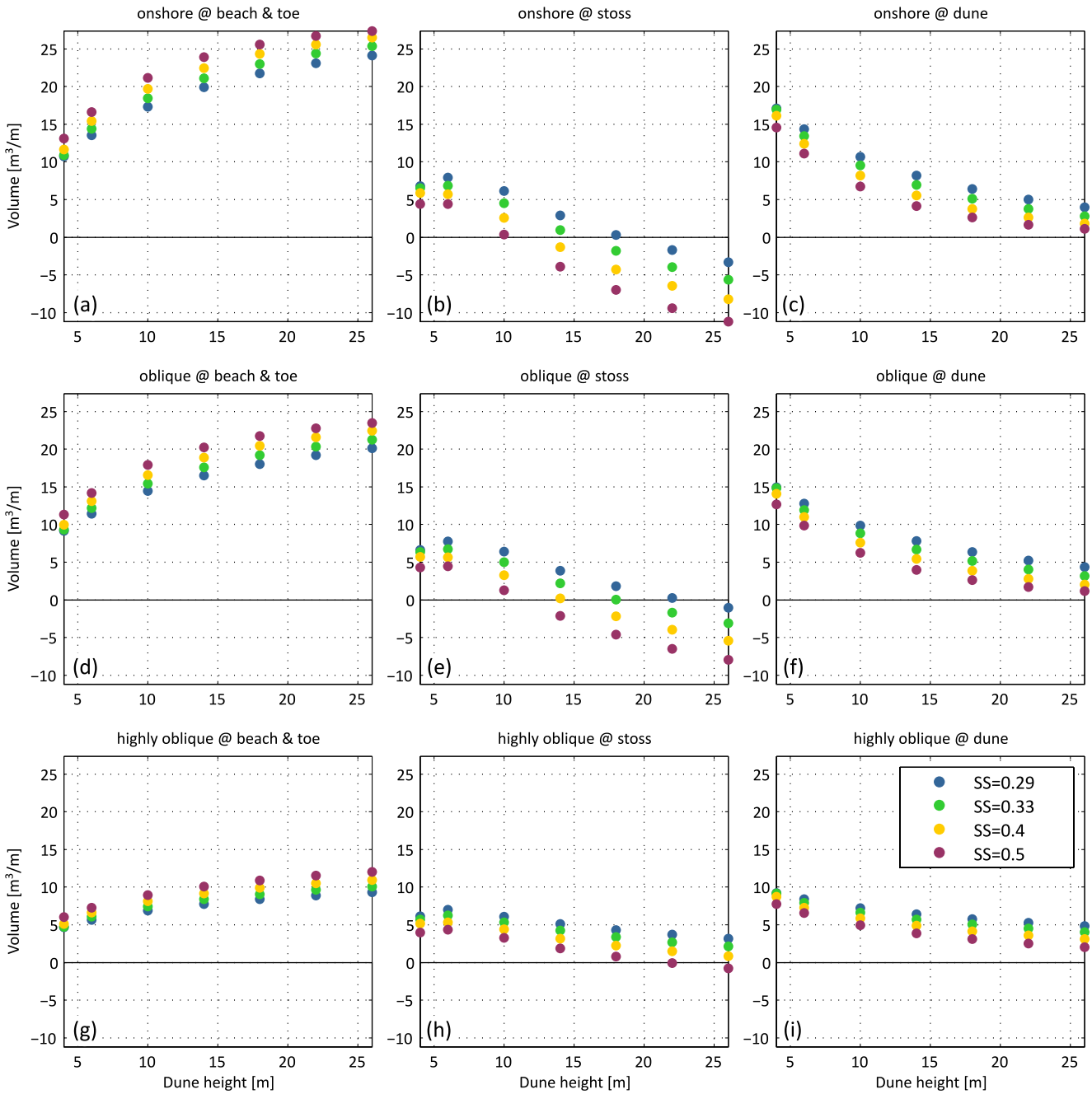

Figure 6. Variability of volume change (y axis, in m^3/m) with dune height (x axis, in m), at the beach up to the dune toe (left (a), (d), and (g)), at the dune stoss (toe to crest; center, (b), (e), and (h)) and the entire dune (toe to lee; right, (c), (f), and (i)) for onshore (top, (a)–(c); 0°–15°), oblique (middle, (d)–(f); 15°–45°) and highly oblique (bottom, (g)–(i); 45°–75°) winds and for the 4 stoss slopes (SS; values in legend) tested for the case of NL conditions (beach width of 200 m).

influence of stoss slope appears secondary compared to the impact of dune height, as also noted in the flow experiments. Details on the fit of these results to Equation 5, where X denotes sand volume, are given in Table 3.

From the results of the NL transport experiments, it appears that increasing wind incidence angles affect the total accumulation at the dune differently for low and high dunes. For example, and considering a stoss slope of 0.33, the volumes accumulated in a 4-m dune under onshore, oblique and highly oblique winds are 16.9, 14.8, and 9.2 m^3/m, whereas the corresponding values for a 26-m dune are 3.8, 4.0, and 4.5 m^3/m (Figures 6c, 6f, and 6i). Generally, the results indicate that an increase in wind direction for low dunes results to strong decrease of sand transfer to the dune, whereas for high dunes the relative decrease is significantly milder, or even leading to slight

21699011, 2023, 9, Downloaded from https://agupubs.onlinelibrary.wiley.com/doi/10.1029/2023JF007080 by Cochrane Portugal, Wiley Online Library on [06/11/2023]. See the Terms and Conditions (https://onlinelibrary.wiley.com/terms-and-conditions) on Wiley Online Library for rules of use; OA articles are governed by the applicable Creative Commons License

21699011, 2023, 9, Downloaded from https://agupubs.onlinelibrary.wiley.com/doi/10.1029/2023JF007080 by Cochrane Portugal, Wiley Online Library on [06/11/2023]. See the Terms and Conditions (https://onlinelibrary.wiley.com/terms-and-conditions) on Wiley Online Library for rules of use; OA articles are governed by the applicable Creative Commons License

increase in accumulation for higher incidence angles. In fact, the difference in dune accumulation volumes in the NL simulations between consecutive wind bins increases asymptotically to near-zero and/or low positive values for dune heights over 14 m (see differences given in Table S1 of the Supporting Information S1). This points to a critical dune height, beyond which a change in wind direction has little to no impact on sand transfer to the dune.

There is little doubt that the simulated deceleration and acceleration of the flow is very important to the morphological changes that the model predicts. As noted in the Wind2 validation experiment, the wind parameterization may tend to overestimate the influence of topography on the flow, especially for higher wind angles. To assess the impact of such an overestimation on the results analyzed, the NL simulation was repeated, reducing the values predicted by the Kroy parameterization by the error identified in the Wind2 experiment. More specifically, the nondimensional velocity outputs of the Kroy parameterization (initial topography-flow interaction) were multiplied by a reduction factor equal to 1 minus the velocity overestimation. The latter was set equal to the nondimensional velocity RMSE, assessed in Wind2 (Figure 2), thus varying from 0.11 at the toe to 0.22 at the crest, assuming linear variability between the two over the stoss. Windwards from the toe, and over the flow deceleration zone predicted by Kroy, the reduction factor was linearly interpolated between the RMSE at the toe and a reduction factor of 1, set at the most windward grid cell where Kroy predicted undisturbed velocities (nondimensional velocity of 1). Leewards from the crest, the reduction factor was assumed to be 1 at the base of the lee and the values between the crest windward limit and the base of the lee were, again, interpolated linearly. The results of the simulation are provided in Figures S3 and S4 of the Supporting Information S1 (in Figure S3 of the Supporting Information S1 as results of the reduced Kroy run and their difference with the initial NL run; in Figure S4 of the Supporting Information S1 as difference in simulated elevation change along the dune of the initial and the reduced Kroy runs) and show that the changes to the modeled acceleration and deceleration by the topography are relatively low and do not affect the previously mentioned patterns and shifts (e.g., stable to eroding stoss takes place at the same dune heights). Even assuming that the difference of the two runs is a systematic error of the simplified model, inherent in all simulations, the results show that its influence decreases asymptotically to 0 with increasing dune height, meaning that it becomes less important the higher/steeper the topography. The peak difference in volume change for the NL transport experiment (onshore winds) is 7.4 m^3/m at the toe for the lowest/mildest dune and reducing to 0.7 m^3/m for the highest/steepest dune. The related values at the crest are from −6.7 to −0.75 m^3/m, while over the stoss the differences range from −2 to +6.7 m^3/m.

Notably, the changes in topography identified in the lower dunes (height 4 and 8 m; Figure S4 in Supporting Information S1) show an overestimation of the topographic change throughout the profile, whereas all other dune heights show overestimation at the dune toe, underestimation at the crest and overestimation leeward from the crest brink. Considering that we used the RMSE from a 20-m dune (Wind2) in all dune morphologies and that the results of the Wind1 experiment (8-m height) showed lower errors than the ones assumed here, the actual overestimation of the influence of topography is probably exaggerated, especially for low dunes. Though it is likely that the actual sediment transfer to high dunes is overestimated by the model, given that the shifts between erosive and stable conditions over the dune stoss and the variability of volumes change with dune dimensions and wind directions remained consistent with the NL experiments, the patterns identified remain valid.

3.2.3. Influence of Dune Morphology on Sediment Accumulation for Fetch-Limited Conditions

To assess the influence of the fetch effect on the sand accumulation patterns identified for NL conditions, the simulations were repeated considering reduced beach width (FL experiments; see Table 2 for data). The results of FL transport are given in Figure 7, using the same structure and axes limits as the NL run (Figure 6), to allow for direct comparisons. The reduction of total accumulation in the domain compared to the NL case (not shown) dissipates with increasing wind incidence angles due to increasing projected beach widths. The total sand deficit of FL relative to NL transport ranges from 38.5% to 68% (for lowest dune height and slope to highest, respectively) for onshore winds, from 29.7% to 60.4% for oblique winds and from 5.2% to 28.9% for highly oblique winds.

Accumulation along the beach and toe (Figures 7a, 7d, and 7g) shows very little variability with wind incidence, with values between 3.5 and 8.4 m^3/m. Compared to NL conditions (Figures 6a, 6d, and 6g), volumes at the toe are strongly reduced, on average by −68.6% ± 3.4% for onshore, −62.4% ± 4.1% for oblique and −29.7% ± 8.8% for highly oblique winds. Volume changes over the stoss range between −11 and 6.2 m^3/m for onshore winds (Figure 7b), −7.6–6.9 m^3/m for oblique winds (Figure 7e) and −0.5–7.1 m^3/m for highly oblique winds (Figure 7h). These values are very close to the ones simulated for the NL conditions (peak deficit values

21699011, 2023, 9, Downloaded from https://agupubs.onlinelibrary.wiley.com/doi/10.1029/2023JF007080 by Cochrane Portugal, Wiley Online Library on [06/11/2023]. See the Terms and Conditions (https://onlinelibrary.wiley.com/terms-and-conditions) on Wiley Online Library for rules of use; OA articles are governed by the applicable Creative Commons License

for FL: 1.8, 1.2, and 0.3 m^3/m for onshore, oblique and highly oblique winds), with the differences dropping to near-zero for high/steep dunes. Similarly, the volume changes predicted over the dune (Figures 7c, 7f, and 7i) are close to the NL case (Figures 6c, 6f, and 6i). The sand deficit (FL relative to NL) over the dune is therefore also low, with peak volume reduction of -4 m^3/m for onshore winds, -2.1 m^3/m for oblique winds and -0.4 m^3/m for highly oblique winds. The highest deficit is noted for low dunes, while for dune heights over 14 m the changes are negligible.

Essentially, the results show a bimodal dune response to fetch limitation with increasing dune height, with the shift from one mode to the other occurring around the height of 10–14 m. In low dunes, the sediment deficit is distributed to the entire dune, while in higher dunes, the deficit is noted only near the toe and the rest of the dune shows little change between the two conditions. The latter is due to the sediment eroded from the stoss and transferred to the crest and lee (sand recycling) for high dunes, occurring even in conditions of maximum input from the beach. The influence of increasing wind incidence angles on sand transfer to the dune, noted in NL conditions, is also present for the FL case (see differences given in Table S1 of the Supporting Information S1). A change from onshore to oblique winds induces low reduction only to very low dunes of 4–6 m, with the remaining morphologies showing near-zero to low positive values. An increase in wind angle from oblique to highly oblique winds results in reduced sediment transfer to dunes lower than 10–18 m. Therefore, comparing the FL and NL results, fetch limitation appears to draw the critical dune height (beyond which sand transfer to the dune does not change with wind incidence) toward lower dunes, compared to non-limited transport conditions. In terms of variability with the dune shape parameters, details on the fit of the FL results of Figure 7 to Equation 5 are given in Table 3.

3.2.4. Influence of Vegetation on Sediment Accumulation

Both the NL and FL experiments identified erosive conditions along the stoss, with the shift from accumulation to stoss erosion occurring at the same dune dimensions (e.g., for onshore winds, between height of 10 m with slope of 0.5, to height of 18 m with slope of 0.29; Figures 6b, 6e, and 6h and Figures 7b, 7e, and 7h). This shift leads to enhanced sand transfer toward the crest and lee by recycled sand from the stoss and a landward migration of the crest in both cases. This is demonstrated in the indicative profiles given in Figure 8, showing strong differences in accumulation areas between a low/mild dune (4 m/0.29; Figures 8a–8c) and a high/steep dune (14 m/0.5; Figures 8d–8f). It is noted that the height of 14 m was selected to facilitate visualization of vertical change and that higher dunes show similar changes. Given that vegetation density is a critical factor in determining if and when erosive conditions and landward migration of the dune take place, profiles considering low, high and very high density (LD, HD, and VHD; see Table 2 for data) are shown. It is noted that a reduction from HD to LD results to changes in accumulation within the dune (e.g., Figure S5 in Supporting Information S1 shows volumes of LD NL and HD NL at toe and dune are unaffected; similar volume differences are obtained comparing LD FL and LD FL).

For the low dune morphology (Figures 8a–8c), all densities and beach width conditions tested predict stable conditions of growth (vertical accretion at the crest and progradation of the stoss slope). As indicated previously, the changes due to fetch limitation are very high at the dune toe and lower stoss, with small but noticeable differences in the reduction of transport distributed to the rest of the profile for onshore and oblique winds (e.g., FL HD vs. NL HD in Figures 8a and 8b). The influence of density becomes most important near the crest, where higher values retain more sand along the stoss slope and the crest and transport less toward the lee (e.g., NL VHD vs. NL LD in Figures 8a–8c). The influence is more pronounced for onshore than for highly oblique winds.

For the high dune (Figures 8d–8f), beach widths affect accumulation along the toe and the lower stoss, with no changes between NL and FL profiles near the crest. Among the densities considered, only the VHD predicts a stable stoss slope, with LD and HD to simulate stoss erosion, sand transfer toward the lee and landward migration. A density reduction from HD to LD causes more erosion of the stoss and higher landward migration, whereas an increase from HD to VHD manages to stabilize the stoss, with negligible accumulation at the crest and lee. The landward sand transfer and migration rates decrease with increasing wind incidence angles (Figures 8d–8f).

As expected, the simulated morphological changes within the dune are highly linked to the considered vegetation density. Given that the change due to the fetch effect had little impact to the sand transport over the stoss and the crest and lee, we further analyze the impacts of vegetation density focusing on the NL case, assuming that FL conditions have similar behavior. The influence of vegetation coverage (VHD, HD, and LD) on the modeled

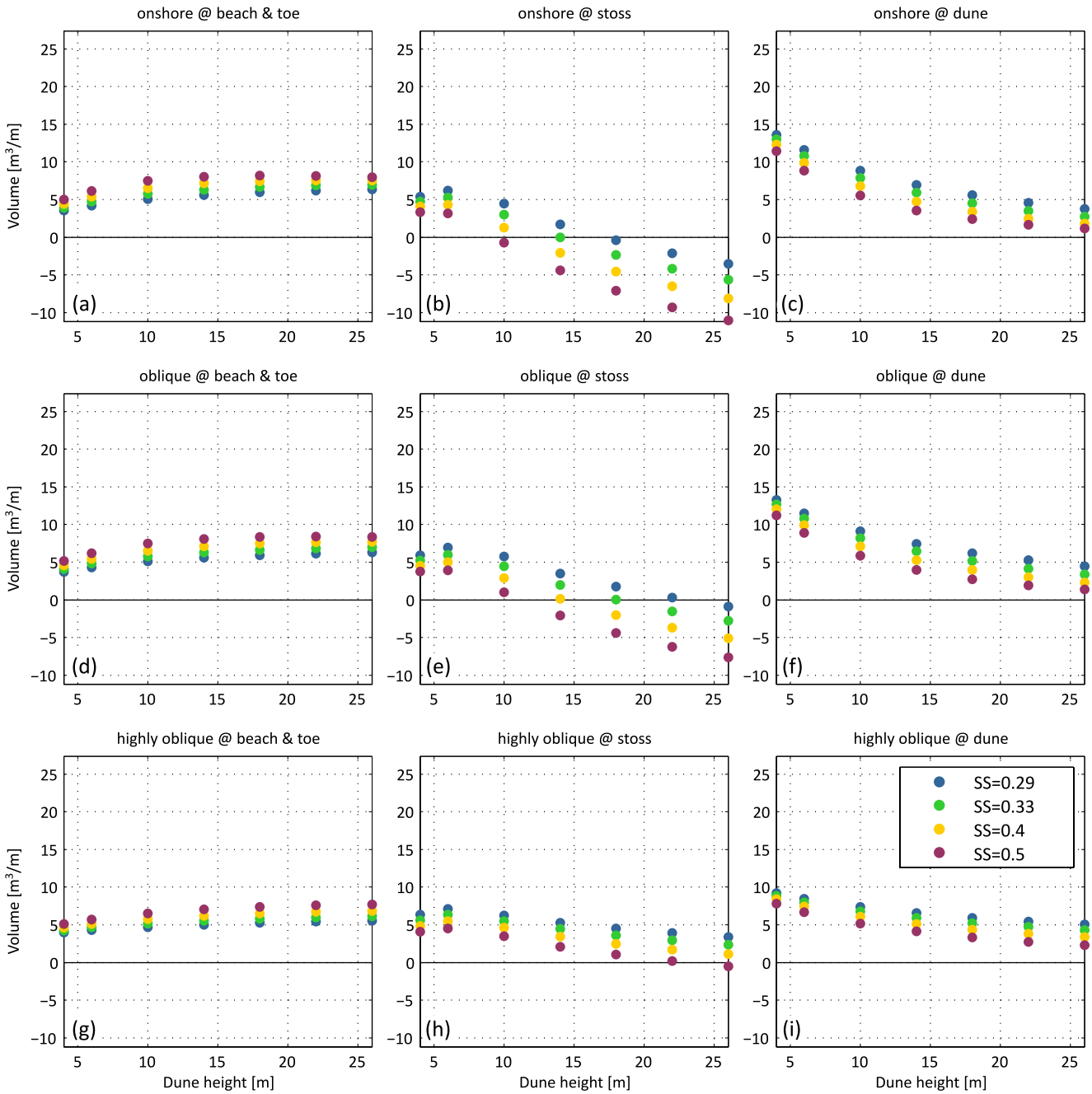

Figure 7. Variability of volume change (y axis, in m^3/m) with dune height (x axis, in m), at the beach up to the dune toe (left, (a), (d), and (g)), at the dune stoss (toe to crest; center, (b), (e), and (h)) and the entire dune (stoss crest and lee; right; (c), (f), and (i)) for onshore (top, (a)–(c); 0°–15°), oblique (middle, (d)–(f); 15°–45°) and highly oblique (bottom, (g)–(i); 45°–75°) winds and for the 4 stoss slopes (SS; legend) tested for the case of FL conditions (beach width of 50 m). The axes limits are the same as the NL transport experiments (Figure 6) to facilitate comparisons.

sand distribution within the dune (stoss and crest-lee) for NL transport conditions is summarized in Figure 9. Volume changes over the stoss slope for the three densities considered are given at the top panels of the plot (Figures 9a–9c; see legend). The related changes over the crest and lee are given in the lower plots, with LD shown in Figures 9d–9f, HD shown in Figures 9g–9i and VHD shown in Figures 9j–9l. These changes are given as "total" and "new" sand, with the latter corresponding to matter originating from the beach. In cases where the stoss slope is stable, the two series overlap, whereas in cases where the stoss is erosive, the two series diverge, with their difference (total-new) being equal to the amount of sand recycled (eroded) from the stoss. As in previ-

21699011, 2023, 9, Downloaded from https://agupubs.onlinelibrary.wiley.com/doi/10.1029/2023JF007080 by Cochrane Portugal, Wiley Online Library on [06/11/2023]. See the Terms and Conditions (https://onlinelibrary.wiley.com/terms-and-conditions) on Wiley Online Library for rules of use; OA articles are governed by the applicable Creative Commons License

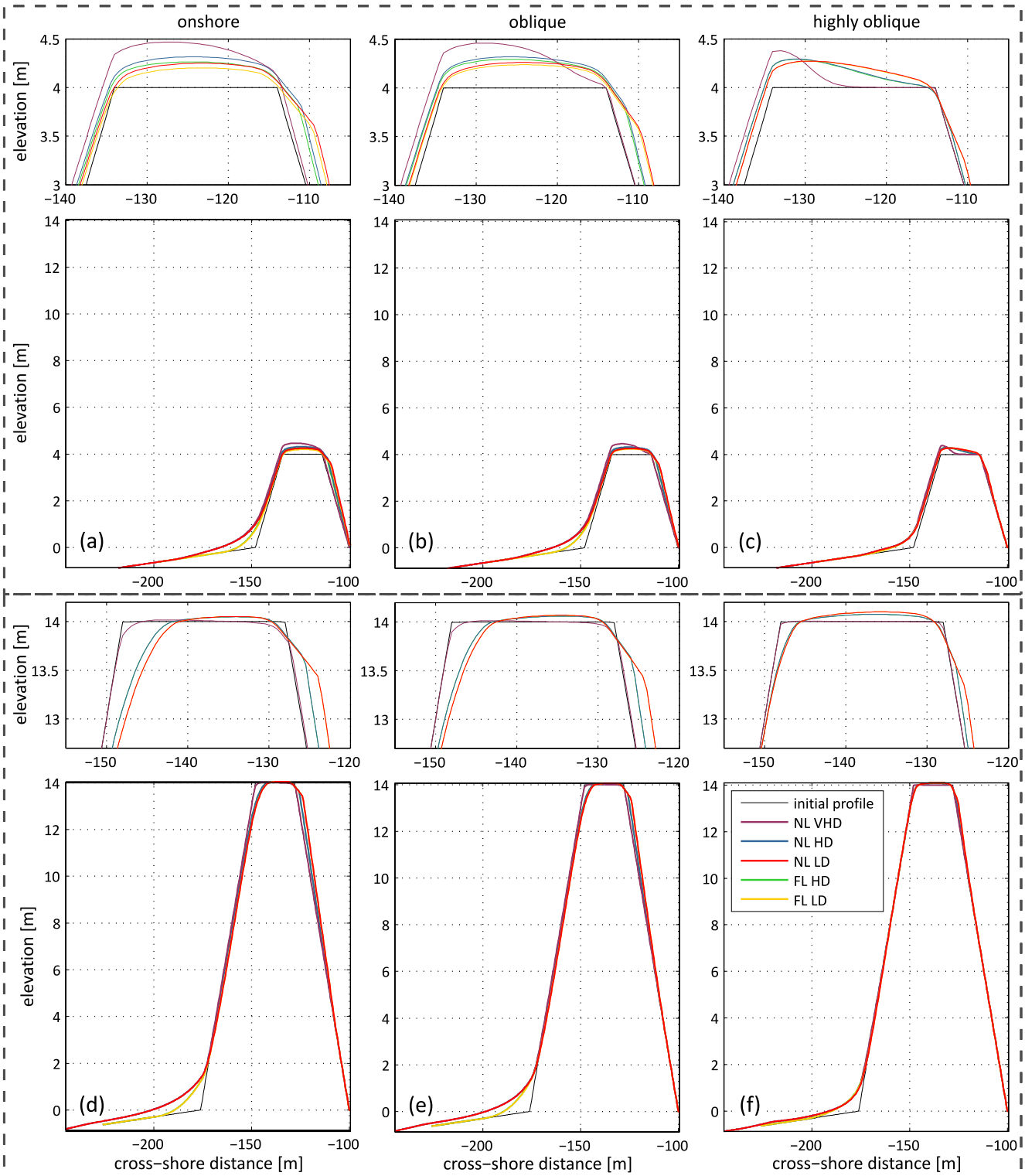

Figure 8. Profile changes for two different dune morphologies and for non-limited (NL) and fetch-limited (FL) conditions and considering very high, high and low vegetation densities (VHD, HD, and LD; legend): top panel ((a)–(c)) shows the case of a low (4 m) and mild-sloped (0.29) dune and bottom panel ((d)–(f)) the case of a high (14 m) and steep (0.5) dune; a zoom of the profiles near the crest is given at the top of each panel (green and blue curves and red and yellow curves overlap for the high dune case; the axes scales of the zoomed plots are the same). Changes are shown for onshore (left; (a) and (d)), oblique (middle; (b) and (e)) and highly oblique (right; (c) and (f)) winds.

21699011, 2023, 9, Downloaded from https://agupubs.onlinelibrary.wiley.com/doi/10.1029/2023JF007080 by Cochrane Portugal, Wiley Online Library on [06/11/2023]. See the Terms and Conditions (https://onlinelibrary.wiley.com/terms-and-conditions) on Wiley Online Library for rules of use; OA articles are governed by the applicable Creative Commons License

ous multipaneled plots, columns from left to right correspond to increasing wind incidence, from onshore to highly oblique winds.

Expectedly, the results show a reducing ability to maintain the position of the stoss with reducing plant density (Figures 9a–9c; VHD to HD to LD; filled triangles, non-filled squares and filled stars, respectively). Only the VHD experiments maintain the position of the stoss (net accumulation for all morphologies) under onshore winds, while stoss erosion increases with reducing density (HD to LD). As wind angles increase, the modeled stoss erosion attenuates, with only very high/steep dunes with LD (height over 14 m for slope of 0.4 and over 18 m for slope of 0.5) to show erosion for highly oblique winds (Figure 9c).

Regarding sand transfer to the crest and lee (Figures 9d–9l), the new sand, introduced from the beach, follows the overall trend of reduction with dune height, stoss slope and wind incidence angle, for all density experiments. The transfer of new sand to the crest and lee between the HD and LD experiments is very similar and appears to be mainly controlled by wind flow. The series of new and total sand for HD and LD begin to diverge around the dune height of 10 m (Figures 9d–9f and Figures 9g–9i) with the introduction of remobilized sand from the stoss. For lower dunes, all density runs show accumulation along the stoss (Figures 9a–9c), with low differences over the crest-lee between density experiments. For higher dunes, the total sand transfer to the crest and lee under the LD scenario is around double the volume simulated under the HD scenario (Figures 9d–9f vs. Figures 9g–9i). For the VHD run, the strong retention of sand along the stoss translates to decreased volumes reaching the crest in all morphologies, dropping to near-zero values for dunes over 10 m. Compared to the new sand delivered to the crest from the HD runs, the VHD volumes are reduced by −0.6 to −6 m^3/m (−14% to −98%; Figures 9g and 9j) for onshore winds and by −0.75 to −2.5 m^3/m (−22% to −99%; Figures 9i and 9l) for highly oblique winds. The results and behavior noted by the HD and LD runs for high dunes (here exceeding 10 m) are consistent with the expected response of a moderately to sparsely vegetated dune, showing signs of landward migration, while the VHD run can be paralleled to the growth patterns of a densely vegetated, fixed dune.

The shift from a fixed dune to a landward migrating dune is highly linked to the presence of vegetation and therefore to the damping of the flow by vegetation considered (see Equation 4). As expected, the sensitivity of the model to the considered wind flow attenuation along the vegetated dune is high. Sensitivity experiments were performed to assess the variability of simulated elevation change along the vegetated dune, induced by a change of ±20% of the flow damping, relative to the HD run (Figure S6 in Supporting Information S1). Reduced damping causes peak reduction of accumulation of −0.6 m at the upper stoss and corresponding increase of +1.2 m at the crest brink (for SS = 0.5 and onshore winds). Conversely, increased damping translates to maximum increase of accumulation at the upper stoss of +0.4 m and reduced accumulation at the brink of −0.7 m. In terms of volume change (Table S2 in Supporting Information S1), the variability over the stoss is within −44.03% ± 7.02% and +23.30% ± 4.72% (onshore winds, peak dune height and averaged stoss slopes), with related changes in the crest and lee between +44.66% ± 7.10% and −23.62% ± 4.74%. Changes in the beach and toe (and over the dune as a whole) are negligible (below 2%).

4. Discussion

The reproduction of wind flow along the windward side of the dune profile, as shown by the calibration (against CFD model) and validation (against field data) experiments, was improved after grid rotation for angled wind incidence, and projection of the profile onto the rotated grid. Given the good agreement between model results and the field data from Schwarz et al. (2021), simulated flow patterns along the foredune slope are aligned with their findings. Building on this, the idealized experiments conducted allowed to identify flow acceleration and deceleration patterns related with wind incidence and dune characteristics (height, stoss slope). Overall, wind speed-down at the toe and speed-up at the stoss and the crest varies logarithmically with dune height and linearly with stoss slope. Results show that the highest topographically forced flow acceleration occurs for directly onshore winds, with peak acceleration near the foredune crest, as also observed by Hesp et al. (2015). The attenuation of the influence of dune topography on the flow with increasing wind incidence angles and the related acceleration and deceleration patterns are also in agreement with previous works (Arens et al., 1995; Hesp et al., 2015; Schwarz et al., 2021; Walker et al., 2009). Results also align with previous findings that dune height is perhaps more important than stoss slope in controlling near-surface flow response over dunes, and particularly at the crest (Hesp et al., 2015; Parsons et al., 2004).

21699011, 2023, 9, Downloaded from https://agupubs.onlinelibrary.wiley.com/doi/10.1029/2023JF007080 by Cochrane Portugal, Wiley Online Library on [06/11/2023]. See the Terms and Conditions (https://onlinelibrary.wiley.com/terms-and-conditions) on Wiley Online Library for rules of use; OA articles are governed by the applicable Creative Commons License

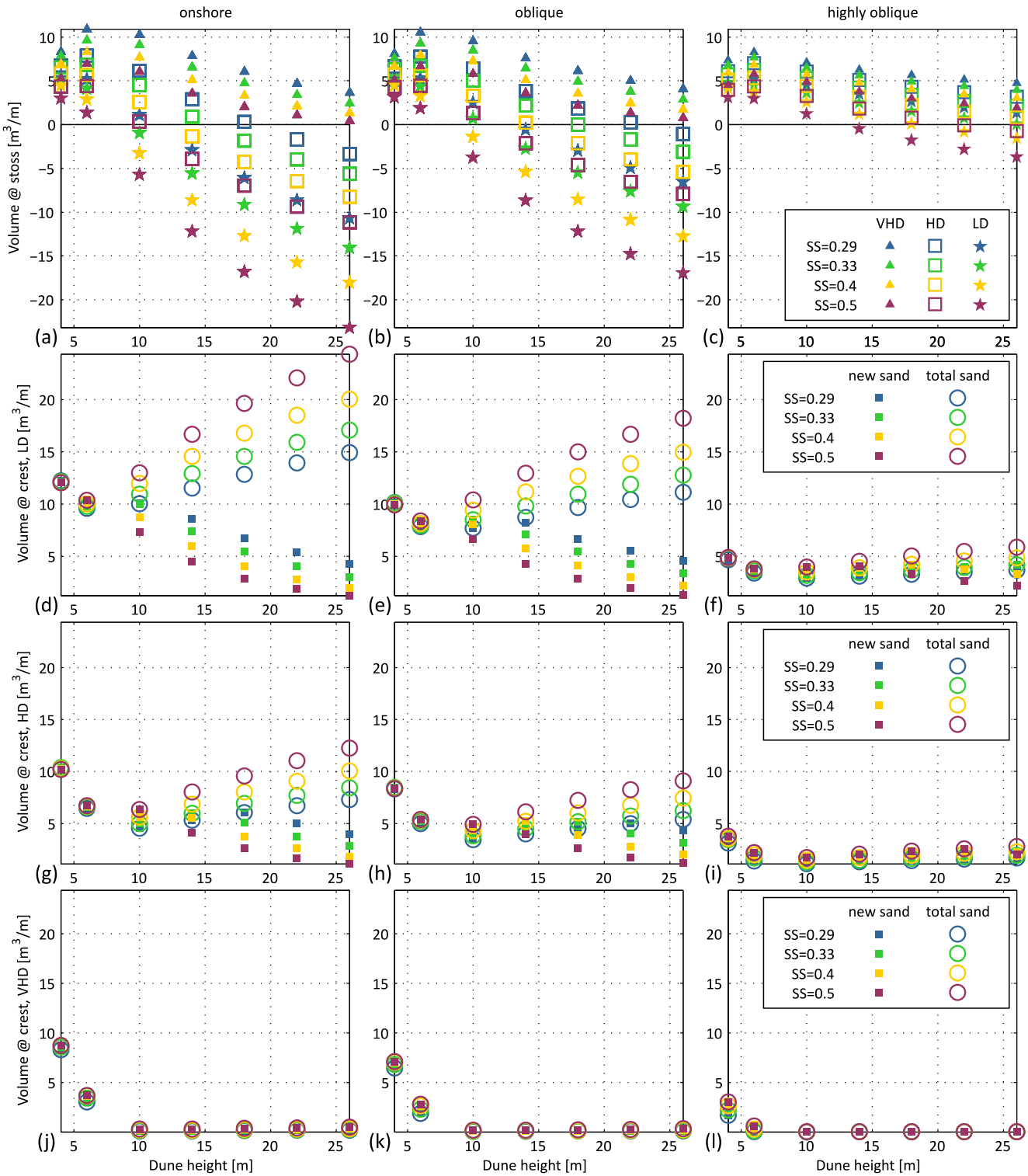

Figure 9. Comparison of volume change within the dune between vegetation density runs for non-limited conditions: volume change at the stoss slope for VHD, HD and LD ((a)–(c); filled triangles, non-filled squares and filled stars, respectively), and total and new (from the beach) sand volumes delivered to the crest (non-filled circles and filled squares, respectively) for LD ((d)–(f)), HD ((g)–(i)) and VHD ((j)–(l)). From left to right the columns show variability for onshore ((a), (d), (g), and (j)), oblique ((b), (e), (h), and (k)) and highly oblique winds ((c), (f), (i), and (l)); note that even though the vertical axes limits are different between volume changes at the stoss (top panel) and at the crest (three lower panels), the axis scale is maintained.

21699011, 2023, 9, Downloaded from https://agupubs.onlinelibrary.wiley.com/doi/10.1029/2023JF007080 by Cochrane Portugal, Wiley Online Library on [06/11/2023]. See the Terms and Conditions (https://onlinelibrary.wiley.com/terms-and-conditions) on Wiley Online Library for rules of use; OA articles are governed by the applicable Creative Commons License

Field data by Arens et al. (1995) show a maximum speed-up increase at the crest from 1.1 to 1.5 for an increase in foredune height from 6 to 10 m (and stoss slope of 1:12 to 1:4), values that compare well with modeled acceleration from the idealized experiments. At a 15-m-high, steep (~30°), unvegetated dune slope (Salmon Hole, SE. Australia), Davidson et al. (2022) measured an increase of 1.83 for near-onshore winds and of 1.54 for oblique winds at the crest, values close to the simulated speed-up of 1.65 and 1.58 for these conditions. Near the middle of the stoss slope, their data show acceleration between 1.25 and 1.13, again comparing well with simulated values between 1.26 and 1.2. At the toe they report a reduction of 0.77–0.81, while modeled values are around 0.5 for both wind incidence angles. Garès and Pease (2015) measured maximum acceleration at the crest of a foredune ridge (of 7.5 m height and 0.45 stoss slope) between 1.65 and 1.4 for onshore to oblique incidence angles. The corresponding modeled acceleration at the crest is 1.5 and 1.43, respectively. Walker et al. (2009) measured average acceleration at the foredune crest (height 8.7 m, stoss slope 0.49) of 1.57 during a highly oblique wind event and of 1.61 during a period of oblique and onshore winds. The corresponding modeled results are 1.3 and 1.48 to 1.55, respectively. Given the degree of alongshore non-uniformity and the strong deviations from the simplified modeled profile in some of these sites—for example, the transect of Davidson et al. (2022) is backed by a blowout with a landward depositional lobe; the measurements of Garès and Pease (2015) were adjacent to a blowout trough -, the agreement with modeled results is considered highly satisfactory.

The main patterns in aeolian sand accumulation (dV, plotted on *y*-axes) with dune morphological parameters, wind incidence and potential limiting conditions, identified from the results of the numerical experiments, are summarized in Figure 10. The top panel shows the influence of fetch length on sand accumulation on the beach (windward of the dune toe) and on the dune (leeward of the dune toe) and its variability with dune height, stoss slope (plotted on *x*-axes) and wind incidence (shown as lines in plots). The bottom panel outlines the influence of vegetation density on the volume changes within the dune parts, for variable dune heights and wind incidence. Essentially, the variability of volume gains within the dune of the top panel (dashed rectangles in Figure 10) is split here into the zones of stoss slope and dune crest and lee, for sparse and densely vegetated dunes. These patterns are explained and discussed in the following paragraphs.

Overall, the sand transport experiments indicate the presence of a logarithmic relation between accumulation and dune height and a linear relation with stoss slope, increasing at the dune toe and decreasing at the dune stoss and crest-lee. Differences in volume changes between onshore and oblique winds were low (reduction of ~14%) in all experiments, in agreement with the observations of R. Davidson-Arnott et al. (2018) over the stoss for different beach conditions. Sand transfer at the toe under NL conditions and highly oblique winds (~60°) is reduced by around 50%, compared to onshore wind incidence. The latter is in accordance with the cosine effect (Bauer & Davidson-Arnott, 2003; Delgado-Fernandez, 2010), showing successful reproduction of the effect by the model, indirectly parameterized by the grid rotation approach. Under FL conditions, the cosine and fetch effects can both affect the accumulation at the toe. There is a tendency for overlapping accumulation volumes at the toe between the different wind bins for low beach widths (Figure 10). Under such conditions, fetch limitation dominates the onshore winds and cosine limitation dominates the highly oblique winds. This is in line with previous research, supporting that even though sand transport may be reduced by the cosine effect for highly oblique winds, the actual transport in narrow beaches may be greater than for onshore winds (Arens, 1996; R. Davidson-Arnott et al., 2018; Delgado-Fernandez, 2010). As beach widths increase, there is increasing separation of accumulation at the toe between wind bins, until NL transport is reached for onshore winds, with reduced accumulation by around 50% (cosine effect) for highly oblique winds (Figure 10).

Regarding the accumulation at the dune (landwards from the dune toe), the results show a relation between the dune morphological characteristics and the wind incidence angles. The difference induced to the sand transfer to the dune by an increase in wind obliquity is smaller when the dune is higher and/or steeper. For low dunes, maximum sand transfer to the dune takes place under shore-normal winds, while beyond a critical dune height, that depends on the considered wind (speeds between 5.40 and 22.72 m/s and average of 12.92 ± 2.34 m/s) and beach conditions (~14–18 m for NL; beach width of 200 m), the balance flips to highly oblique winds. It follows that, above a critical dune height ($DH_{cr,ext}$ in Figure 10), highly oblique winds appear to transfer more sand to the dune than onshore winds. Beach width is also relevant to this pattern, with a tendency to lower the critical dune height value ($DH_{cr,ext}$) as the beach width decreases (i.e., from NL to FL conditions). For example, and assuming a mean value for the stoss slope, the critical dune height value for NL conditions (Figure 6) is around 18.5 m and it reduces to 14.6 m for FL conditions (Figure 7; beach width of 50 m). Therefore, the balance in sand transfer

21699011, 2023, 9, Downloaded from https://agupubs.onlinelibrary.wiley.com/doi/10.1029/2023JF007080 by Cochrane Portugal, Wiley Online Library on [06/11/2023]. See the Terms and Conditions (https://onlinelibrary.wiley.com/terms-and-conditions) on Wiley Online Library for rules of use; OA articles are governed by the applicable Creative Commons License

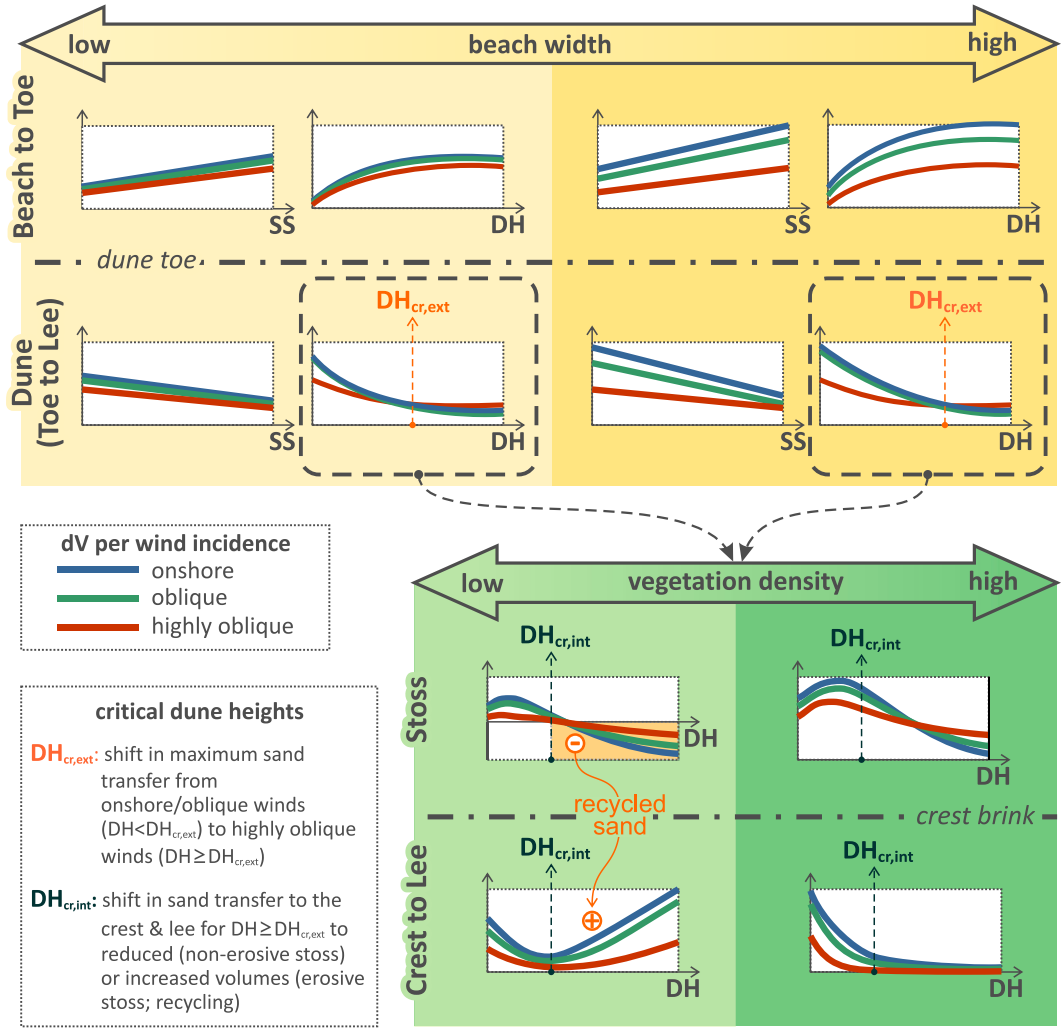

Figure 10. Schematic representation of dependencies between sand volume change (dV; all *y*-axes), dune morphology (DH: dune height, SS: stoss slope; in *x*-axes) and wind incidence (line colors; see legend). The top (yellow) panel shows the influence of beach width (narrow to wide beach conditions; left to right) on the variability of dV with stoss slope (SS) and dune height (DH), for the zone windward of the dune toe (beach to toe) and for the dune (toe to lee). The bottom (green) panel shows the impact of vegetation density (sparsely to densely vegetated dunes; left to right) on the distribution of sand volumes within the stoss and the dune crest and lee as a function of DH (splitting the variability of dV with DH in the dune, shown in the top panel and marked with dashed rectangles, into stoss and crest to lee; changes of dV with stoss slope are omitted due to low variability). Critical dune heights noted on the plots are explained in the legend (bottom left); note the negative (erosion; orange-shaded area) volumes for sparsely vegetated dune stoss and DH > $DH_{cri,int}$, that increase accumulation at the crest and lee (sand recycling).

to the dune between wind incidence angles is highly influenced by both the dune height and the beach width: (a) the higher the dune and/or (b) the narrower the beach, the more likely that the highest sand transfer takes place under high incidence angles. These general trends agree with the statement by R. Davidson-Arnott et al. (2018) that sediment can be transferred from the beach to the foredune, even with a steep foredune stoss slope, primarily because much of the sediment transfer takes place under oblique rather than onshore winds. The importance of variations in beach width in controlling rates of sediment supply to the foredune has been stressed by R. G. D. Davidson-Arnott and Law (1996), who postulated that in cases of narrow beaches (widths below 50 m) it exceeds that of wind climate. The trade-off between transport reduction by the cosine effect and transport enhancement by increasing fetch lengths under increasing wind incidence is well documented by previous works (Bauer & Davidson-Arnott, 2003; Delgado-Fernandez, 2010), resulting in transport enhancement across the dune line as the angle of wind approach becomes oblique in narrow beaches.

21699011, 2023, 9, Downloaded from https://agupubs.onlinelibrary.wiley.com/doi/10.1029/2023JF007080 by Cochrane Portugal, Wiley Online Library on [06/11/2023]. See the Terms and Conditions (https://onlinelibrary.wiley.com/terms-and-conditions) on Wiley Online Library for rules of use; OA articles are governed by the applicable Creative Commons License

21699011, 2023, 9, Downloaded from https://agupubs.onlinelibrary.wiley.com/doi/10.1029/2023JF007080 by Cochrane Portugal, Wiley Online Library on [06/11/2023]. See the Terms and Conditions (https://onlinelibrary.wiley.com/terms-and-conditions) on Wiley Online Library for rules of use; OA articles are governed by the applicable Creative Commons License

Changes within the dune itself are highly linked to the conditions of the upwind zone, as well as by wind acceleration and vegetation cover and characteristics (e.g., Cohn et al., 2019; Costas et al., 2023; Durán & Moore, 2013; Hovenga et al., 2023). Simulated high/steep and moderately vegetated dunes show a high degree of sand recycling within the dune (from the stoss slope to the crest and lee; Figure 9). The dune plant parameters considered (density and constant for plant characteristics) vary only slightly along the profile for each experiment. This choice was made to minimize cross-shore variability of the considered vegetation parameters, to avoid localized influences and spurious effects that could potentially skew the results and complicate the comparison between runs and areas and the extraction of general trends. Even though the simplified wind module used may slightly overestimate the impact of topography to the flow for high dunes, sensitivity experiments (Figures S3 and S4 in Supporting Information S1) showed that the accumulation patterns and shifts identified were not impacted. As expected, however, the sensitivity of simulated morphological change within the vegetated part of the domain to the vegetation parameters considered is rather high, as shown by targeted sensitivity experiments (Figure S6; Table S2 in Supporting Information S1) and by the different density values considered in the experiments (Figure 8). So, on one hand, we recognize that whether, and to what extent, sand recycling takes place within the dune is highly dependent on the considered values for the flow attenuation offered by the vegetation. Given that the model performed well in the sand transport calibration experiments, we can say with a high degree of certainty that the vegetation parameterization can be adequately tuned to fit field experiments and reproduce profile changes at event to annual timescales and to reproduce the influence of plant type (i.e., dune builders and burial tolerant and intolerant stabilizers) and growth pattern on the morphology of the dune (Ruggiero et al., 2018) over long-term scales. On the other hand, the aim of the numerical experiments is to investigate dune morphodynamics, and not some form of "universal prediction." Thus, the focus is not on pinpointing a specific dune height beyond which sand recycling occurs (which would be highly reliant on local conditions) but rather to explore its dependences and impacts on dune adaptation. Keeping this in mind, we note that the experiments show the presence of a second critical dune height ($DH_{cr,int}$ in Figure 10), beyond which the sand transferred to the crest and lee either reduces to near-zero due to high retention over the (non-erosive) stoss, or it is mixed with remobilized sand from the (erosive) stoss. The latter case maintains a significant sand transfer to the crest and lee from the beach, even though volumes also reduce with height and steepness. Lower dunes ($<DH_{cr,int}$) continue to grow, irrespective of the considered density.

Thus, the above point to two different types of evolutionary patterns for high dunes: (a) in cases of densely vegetated (enough to maintain the position of the stoss) dunes, the vertical growth practically ceases and the dune progrades seawards; (b) in cases of sparser vegetation the dune retreats landwards, with high sand transfer to the lee. This finding is in agreement with Schwarz et al. (2021), who report decrease in sand flux across the foredune (20 m height, slope 1:2.5), down to 99% at the dune crest compared to the toe, and with similar observations by Arens (1996). Bauer et al. (2022) also reach similar conclusions, after exploring a densely covered dune under oblique moderate winds, stating that sediment transport across the beach leads to deposition at the foredune toe and lower stoss slope, with virtually no sedimentation on the upper stoss or crest (~9 m). The sand transfer from the stoss slope to the crest and lee is in line with the long-term observations of Ollerhead et al. (2013) over a coastal stretch of 5 km in the Greenwich Peninsula (NE coast of Prince Edward Islands, Canada), documenting a landward migrating foredune. Similarly, the morphological evolution of a 4-km long and around 20-m high coastal dune system in Truc Vert (SW France), showing quasi-steady vertical growth and landward migration of the foredune crest between 2011 and 2019, promoted during high-energy wind storms (Laporte-Fauret et al., 2020), is also aligned with the idea that continued sand transfer to a high dune is partially through recycled sand. The experiments showing dune landward migration can be directly related to longer-term dune adaptation schemes, such as the landward dune migration in response to SLR, described by Robin's Rule (R. G. D. Davidson-Arnott, 2005; R. G. D. Davidson-Arnott & Bauer, 2021). Measurements of long-term accretion rates in the Skallingen barrier foredunes (~8 m; SW Denmark) showed sand volume gains on the crest and lee slope that were comparable to beach volume increase by bar welding (Aagaard et al., 2004), similar to the simulated growth pattern for low dunes.

The findings of the analysis regarding the gradual decrease of vertical growth with dune height appear to align with the idea of a "steady-state foredune height", put forward by Durán and Moore (2013), which they attribute to the presence of a negative feedback between topography and wind flow. R. Davidson-Arnott et al. (2018) oppose this hypothesis, stating that "*the rate of growth in foredune height per unit volume increase will decrease over time*, *which gives the perception of an equilibrium height having been reached asymptotically*." Further-

more, they criticize the Durán and Moore (2013) model for using only onshore winds, postulating that a very large proportion of annual total transport into most foredunes takes place under oblique and alongshore winds. Our experiments simulated variable wind directions and the results, expressed in sand volumes (and not vertical change rates), suggest that there is an asymptotic reduction of sand transfer to the dune and of sand reaching landwards from the crest with dune height. As mentioned before, the contribution of highly oblique winds can indeed be higher than that of onshore winds in high dunes; however, the asymptotic reduction with height persists.

Even though our experiments focus on significantly shorter timescales than those of Durán and Moore (2013) and consider a pre-existing vegetated dune, the main drivers and controlling processes are comparable. The use of perpetual winds in both cases raises the question if some form of equilibrium is not pre-conditioned to occur. In our short-term experiments, we opted for using the same wind (moderate to strong) time series to obtain comparable sand transfer conditions from the beach. Still, it can be argued that the work needed to transport the same amount of sand from the beach to the crest should increase with dune height; therefore, an asymptotic behavior is, to some extent, expected. Schwarz et al. (2021) also postulated that the sediment flux at the dune crest is ultimately limited by the wind velocity and the distance traveled over vegetation. These considerations are in line with the remarks of Houser et al. (2022) that the repetition and recurrence of surf and aeolian processes lead to the observation of similar beach-dune profiles, while individual foredune topographies can deviate from what may appear as an equilibrium profile due to site-specific and scale-dependent controls and history.

5. Conclusions

The work presented focuses on investigating dune wind flow and sand transport patterns over simplified foredune morphologies, utilizing recent advances (fetch effect and grid rotation) to the simplified 1-D Duna morphodynamic model. Calibration and validation tests showed that the model: (a) accurately captures the variability in wind flow evolution over the windward side of the dune (stagnation at the toe, gradual acceleration along the stoss slope and peak speed-up at the windward crest brink) for variable wind directions (against both CFD model results and field data); (b) tested against field data from two dune sites (FRF and Praia de Faro), over shorter (35 days for FRF) and longer (1 year for Praia de Faro) timescales, reproduced the vertical changes along both profiles with reasonable accuracy.

Based on the idealized numerical experiments conducted, we can conclude that:

1. There is a generalized pattern of logarithmic change with dune height and linear change with stoss slope, in both wind flow and sand accumulation along the beach (up to the toe), over the dune as a whole (toe to lee) and within dune zones (stoss, crest to lee). Overall, dune height appears as a more important morphological parameter than slope, while its influence on wind speed and elevation change along the profile decreases with increasing wind incidence.
2. Under non-limited fetch conditions, the reduction in sand accumulation by oblique winds, relative to onshore winds, is low (~14%). Comparing highly oblique and onshore winds, sand volumes are reduced by around half, consistently to the cosine effect.
3. Accumulation at the toe (increasing with dune height) is also highly influenced by beach width and wind incidence. For narrow beach widths, accumulated sand varies little with wind incidence as transport is limited by the fetch effect for onshore winds and by the cosine effect under high incidence angles. As beach widths increase, there is increasing separation of accumulation volumes at the toe between incidence angles, until maximum accumulation at the toe (non-limited transport) is reached for onshore winds.
4. Sand transfer to the dune (toe to lee) reduces with dune height, while the balance between wind incidence angles is also influenced by beach width. For low dunes, maximum sand transfer to the dune takes place under shore-normal winds, while beyond a critical dune height (depending on beach width) the balance flips to highly oblique winds. Overall, the higher the dune and/or the narrower the beach, the less sediment is transported to the dune and the more likely it is that maximum accumulation takes place under high wind angles.
5. Even though sand transfer to the crest for high dunes (higher than the critical) may continue (i.e., under high incidence angles), the sand volumes are significantly reduced, compared to lower dunes. The variability with dune height asymptotically tends to zero (near-cessation of vertical dune growth), thus supporting the concept of a *maximum dune height*, which is however inextricably linked to the specific forcing/limiting conditions of each site.

21699011, 2023, 9, Downloaded from https://agupubs.onlinelibrary.wiley.com/doi/10.1029/2023JF007080 by Cochrane Portugal, Wiley Online Library on [06/11/2023]. See the Terms and Conditions (https://onlinelibrary.wiley.com/terms-and-conditions) on Wiley Online Library for rules of use; OA articles are governed by the applicable Creative Commons License

21699011, 2023, 9, Downloaded from https://agupubs.onlinelibrary.wiley.com/doi/10.1029/2023JF007080 by Cochrane Portugal, Wiley Online Library on [06/11/2023]. See the Terms and Conditions (https://onlinelibrary.wiley.com/terms-and-conditions) on Wiley Online Library for rules of use; OA articles are governed by the applicable Creative Commons License

6. Results point to two different types of evolutionary pathways for high dunes: either the dune is vegetated enough to maintain the position of the stoss, in which case vertical growth near-ceases and progradation is promoted, or the vegetation is not dense enough and dune retreats landwards, with high sand transfer to the crest and lee, as a mixture of sand transport from the beach and recycled sand from the stoss.

Data Availability Statement

The Duna model is written in Matlab and the code is available under GNU Lesser General Public License v2.1 at https://github.com/danoroelvink/duna. The model outputs presented in the article are provided in the Zenodo repository (Kombiadou et al., 2023): https://doi.org/10.5281/zenodo.8120830.
Data used for calibration/validation are cited in Section 2.2 (and listed in Table 1) and are as follows: UA data and topography for wind flow experiment Wind2 and input coastal wind time series from Schwarz et al. (2020); topographic profiles and input wind time series for experiment Morpho1 were obtained from TDS Catalog (2022).

Acknowledgments
The work is a contribution to the ENLACE project, co-financed by the European Fund for Regional Development-FEDER, through the Algarve Regional Operational Program and National Funds through the Fundação para a Ciência e a Tecnologia (FCT), Portugal, through Grant ALG-01-0145-FEDER-028949 (PTDC/CTA-GFI/28949/2017) and to project CREST, also funded by FCT through Grant 2022.05392.PTDC. KK was supported by the contract CEECINST/00146/2018/CP1493/CT0011 and SC by the contract 2021.04286.CEECIND, both funded by FCT. Authors KK and SC also recognize the support of national funds through FCT, under the project LA/P/0069/2020, granted to the Associate Laboratory ARNET, and UID/00350/2020 granted to CIMA. The authors would also like to thank the Associate Editor, Evan B. Goldstein, and three anonymous reviewers for their contribution in improving the present manuscript.

References

Aagaard, T., Davidson-Arnott, R., Greenwood, B., & Nielsen, J. (2004). Sediment supply from shoreface to dunes: Linking sediment transport measurements and long-term morphological evolution. *Geomorphology*, *60*(1–2), 205–224. https://doi.org/10.1016/J.GEOMORPH.2003.08.002

Arens, S. M. (1996). Patterns of sand transport on vegetated foredunes. *Geomorphology*, *17*(4), 339–350. https://doi.org/10.1016/0169-555X(96)00016-5

Arens, S. M., Van Kaam-Peters, H. M. E., & Van Boxel, J. H. (1995). Air flow over foredunes and implications for sand transport. *Earth Surface Processes and Landforms*, *20*(4), 315–332. https://doi.org/10.1002/ESP.3290200403

Bagnold, R. A. (1936). The movement of desert sand. *Proceedings of the Royal Society of London. Series A—Mathematical and Physical Sciences*, *157*(892), 594–620. https://doi.org/10.1098/RSPA.1936.0218

Bauer, B. O., & Davidson-Arnott, R. G. D. (2003). A general framework for modeling sediment supply to coastal dunes including wind angle, beach geometry, and fetch effects. *Geomorphology*, *49*(1–2), 89–108. https://doi.org/10.1016/S0169-555X(02)00165-4

Bauer, B. O., Hesp, P. A., Smyth, T. A. G., Walker, I. J., Davidson-Arnott, R. G. D., Pickart, A., et al. (2022). Air flow and sediment transport dynamics on a foredune with contrasting vegetation cover. *Earth Surface Processes and Landforms*, *47*(11), 2811–2829. https://doi.org/10.1002/esp.5425

Brier, G. W. (1950). Verification of forecasts expressed in terms of probability. *Monthly Weather Review*, *78*(1), 1–3. https://doi.org/10.1175/1520-0493(1950)078<0001:VOFEIT>2.0.CO;2

Brodie, K., Conery, I., Cohn, N., Spore, N., & Palmsten, M. (2019). Spatial variability of coastal foredune part A: Timescales of months to years. *Journal of Marine Science and Engineering*, *7*(5), 124. https://doi.org/10.3390/jmse7050124

Buckley, R. (1987). The effect of sparse vegetation on the transport of dune sand by wind. *Nature*, *325*(6103), 426–428. https://doi.org/10.1038/325426a0

Charbonneau, B. R., Duarte, A., Swannack, T. M., Johnson, B. D., & Piercy, C. D. (2022). DOONIES: A process-based ecogeomorphological functional community model for coastal dune vegetation and landscape dynamics. *Geomorphology*, *398*, 108037. https://doi.org/10.1016/J.GEOMORPH.2021.108037

Cohn, N., Hoonhout, B., Goldstein, E., De Vries, S., Moore, L., Durán Vinent, O., & Ruggiero, P. (2019). Exploring marine and aeolian controls on coastal foredune growth using a coupled numerical model. *Journal of Marine Science and Engineering*, *7*(1), 13. https://doi.org/10.3390/jmse7010013

Costas, S., de Sousa, L. B., Kombiadou, K., Ferreira, Ó., & Plomaritis, T. A. (2020). Exploring foredune growth capacity in a coarse sandy beach. *Geomorphology*, *371*, 107435. https://doi.org/10.1016/j.geomorph.2020.107435

Costas, S., Gallego-Fernández, J. B., Bon de Sousa, L., & Kombiadou, K. (2023). Ecogeomorphic response of a coastal dune in southern Portugal regulated by extrinsic factors. *Catena*, *221*, 106796. https://doi.org/10.1016/J.CATENA.2022.106796

Costas, S., Kombiadou, K., & Roelvink, D. (2019). How do multiple beach and dune beach ridges emerge and evolve in prograding coasts? In *Proceedings of the 9th international conference on coastal sediments 2019* (pp. 2282–2295). World Scientific Pub Co Pte Lt. https://doi.org/10.1142/9789811204487_0195

Davidson, S. G., Hesp, P. A., DaSilva, M., & Da Silva, G. M. (2022). Flow dynamics over a high, steep, erosional coastal dune slope. *Geomorphology*, *402*, 108111. https://doi.org/10.1016/J.GEOMORPH.2022.108111

Davidson-Arnott, R., Hesp, P., Ollerhead, J., Walker, I., Bauer, B., Delgado-Fernandez, I., & Smyth, T. (2018). Sediment budget controls on foredune height: Comparing simulation model results with field data. *Earth Surface Processes and Landforms*, *43*(9), 1798–1810. https://doi.org/10.1002/ESP.4354

Davidson-Arnott, R. G. D. (2005). Conceptual model of the effects of sea level rise on sandy coasts. *Journal of Coastal Research*, *21*(6), 1166–1172. https://doi.org/10.2112/03-0051.1

Davidson-Arnott, R. G. D., & Bauer, B. O. (2021). Controls on the geomorphic response of beach-dune systems to water level rise. *Journal of Great Lakes Research*, *47*(6), 1594–1612. https://doi.org/10.1016/j.jglr.2021.05.006

Davidson-Arnott, R. G. D., & Law, M. N. (1996). Measurement and prediction of long-term sediment supply to coastal foredunes. *Journal of Coastal Research*, *12*(3), 654–663. Retrieved from https://journals.flvc.org/jcr/article/view/80227

Delgado-Fernandez, I. (2010). A review of the application of the fetch effect to modelling sand supply to coastal foredunes. *Aeolian Research*, *2*(2–3), 61–70. https://doi.org/10.1016/J.AEOLIA.2010.04.001

de M. Luna, M. C. M., Parteli, E. J. R., Durán, O., & Herrmann, H. J. (2011). Model for the genesis of coastal dune fields with vegetation. *Geomorphology*, *129*(3–4), 215–224. https://doi.org/10.1016/j.geomorph.2011.01.024

Durán, O., & Herrmann, H. J. (2006). Vegetation against dune mobility. *Physical Review Letters*, *97*(18), 188001. https://doi.org/10.1103/PHYSREVLETT.97.188001

Durán, O., & Moore, L. J. (2013). Vegetation controls on the maximum size of coastal dunes. *Proceedings of the National Academy of Sciences of the United Sates of America*, *110*(43), 17217–17222. https://doi.org/10.1073/pnas.1307580110

Durán Vinent, O., & Moore, L. J. (2015). Barrier island bistability induced by biophysical interactions. *Nature Climate Change*, *5*(2), 158–162. https://doi.org/10.1038/nclimate2474

Ferreira, Ó., Plomaritis, T. A., & Costas, S. (2019). Effectiveness assessment of risk reduction measures at coastal areas using a decision support system: Findings from Emma storm. *Science of the Total Environment*, *657*, 124–135. https://doi.org/10.1016/j.scitotenv.2018.11.478

Ferreira, O., Viavattene, C., Jiménez, J., Bole, A., Plomaritis, T., Costas, S., & Smets, S. (2016). CRAF Phase 1, a framework to identify coastal hotspots to storm impacts. In *E3S web of conferences* (Vol. 7, p. 11008). EDP Sciences. https://doi.org/10.1051/e3sconf/20160711008

Garès, P. A., & Pease, P. (2015). Influence of topography on wind speed over a coastal dune and blowout system at Jockey's Ridge, NC, USA. *Earth Surface Processes and Landforms*, *40*(7), 853–863. https://doi.org/10.1002/ESP.3670

Garzon, J. L., Costas, S., & Ferreira, O. (2022). Biotic and abiotic factors governing dune response to storm events. *Earth Surface Processes and Landforms*, *47*(4), 1013–1031. https://doi.org/10.1002/esp.5300

Goldstein, E. B., & Moore, L. J. (2016). Stability and bistability in a one-dimensional model of coastal foredune height. *Journal of Geophysical Research: Earth Surface*, *121*(5), 964–977. https://doi.org/10.1002/2015JF003783

Hallin, C., Larson, M., & Hanson, H. (2019). Simulating beach and dune evolution at decadal to centennial scale under rising sea levels. *PLoS One*, *14*(4), e0215651. https://doi.org/10.1371/journal.pone.0215651

Herrero, X., Costas, S., & Kombiadou, K. (2020). Coastal ridge constructive processes at a multi-decadal scale in Barreta Island (southern Portugal). *Earth Surface Processes and Landforms*, *45*(2), 411–423. https://doi.org/10.1002/esp.4742

Hesp, P. A., & Smyth, T. A. G. (2016). Jet flow over foredunes. *Earth Surface Processes and Landforms*, *41*(12), 1727–1735. https://doi.org/10.1002/esp.3945

Hesp, P. A., & Smyth, T. A. G. (2021). CFD flow dynamics over model scarps and slopes. *Physical Geography*, *42*(1), 1–24. https://doi.org/10.1080/02723646.2019.1706215

Hesp, P. A., Smyth, T. A. G., Nielsen, P., Walker, I. J., Bauer, B. O., & Davidson-Arnott, R. (2015). Flow deflection over a foredune. *Geomorphology*, *230*, 64–74. https://doi.org/10.1016/J.GEOMORPH.2014.11.005

Hesp, P. A., Walker, I. J., Chapman, C., Davidson-Arnott, R., & Bauer, B. O. (2013). Aeolian dynamics over a coastal foredune, Prince Edward Island, Canada. *Earth Surface Processes and Landforms*, *38*(13), 1566–1575. https://doi.org/10.1002/ESP.3444

Hesp, P. A., Walker, I. J., Namikas, S. L., Davidson-Arnott, R., Bauer, B. O., & Ollerhead, J. (2009). Storm wind flow over a foredune, Prince Edward Island, Canada. *Journal of Coastal Research*, (SI 56), 312–316.

Hoonhout, B. M., & de Vries, S. (2016). A process-based model for aeolian sediment transport and spatiotemporal varying sediment availability. *Journal of Geophysical Research: Earth Surface*, *121*(8), 1555–1575. https://doi.org/10.1002/2015JF003692

Houser, C. (2013). Alongshore variation in the morphology of coastal dunes: Implications for storm response. *Geomorphology*, *199*, 48–61. https://doi.org/10.1016/j.geomorph.2012.10.035

Houser, C., Smith, A., Lunardi, B., George, E., & Lehner, J. (2022). Textbook dune: Is there a representative and scale-invariant beach-dune profile? *Canadian Geographer/Le Géographe Canadien*, *66*(4), 783–796. https://doi.org/10.1111/CAG.12792

Houser, C., Wernette, P., & Weymer, B. A. (2018). Scale-dependent behavior of the foredune: Implications for barrier island response to storms and sea-level rise. *Geomorphology*, *303*, 362–374. https://doi.org/10.1016/J.GEOMORPH.2017.12.011

Hovenga, P. A., Ruggiero, P., Itzkin, M., Jay, K. R., Moore, L., & Hacker, S. D. (2023). Quantifying the relative influence of coastal foredune growth factors on the U.S. Mid-Atlantic Coast using field observations and the process-based numerical model Windsurf. *Coastal Engineering*, *181*, 104272. https://doi.org/10.1016/j.coastaleng.2022.104272

Itzkin, M., Moore, L. J., Ruggiero, P., & Hacker, S. D. (2020). The effect of sand fencing on the morphology of natural dune systems. *Geomorphology*, *352*, 106995. https://doi.org/10.1016/J.GEOMORPH.2019.106995

Itzkin, M., Moore, L. J., Ruggiero, P., Hovenga, P. A., & Hacker, S. D. (2022). Combining process-based and data-driven approaches to forecast beach and dune change. *Environmental Modelling & Software*, *153*, 105404. https://doi.org/10.1016/J.ENVSOFT.2022.105404

Jackson, D. W. T., Beyers, J. H. M., Lynch, K., Cooper, J. A. G., Baas, A. C. W., & Delgado-Fernandez, I. (2011). Investigation of three-dimensional wind flow behaviour over coastal dune morphology under offshore winds using computational fluid dynamics (CFD) and ultrasonic anemometry. *Earth Surface Processes and Landforms*, *36*(8), 1113–1124. https://doi.org/10.1002/ESP.2139

Keijsers, J. G. S., De Groot, A. V., & Riksen, M. J. P. M. (2016). Modeling the biogeomorphic evolution of coastal dunes in response to climate change. *Journal of Geophysical Research: Earth Surface*, *121*(6), 1161–1181. https://doi.org/10.1002/2015JF003815

Kombiadou, K., Costas, S., & Roelvink, D. (2021). Simulating destructive and 1247 constructive morphodynamic processes in steep beaches. *Journal of Marine Science 1248 and Engineering*, *9*(1), 86. https://doi.org/10.3390/JMSE9010086

Kombiadou, K., Costas, S., & Roelvink, D. (2023). Exploring controls on coastal dune growth through a simplified model [Dataset]. Zenodo. https://doi.org/10.5281/zenodo.8120830

Kroy, K., Sauermann, G., & Herrmann, H. J. (2002a). Minimal model for aeolian sand dunes. *Physical Review E—Statistical Physics, Plasmas, Fluids, and Related Interdisciplinary Topics*, *66*(3), 031302. https://doi.org/10.1103/PhysRevE.66.031302

Kroy, K., Sauermann, G., & Herrmann, H. J. (2002b). Minimal model for sand dunes. *Physical Review Letters*, *88*(5), 543011–543014. https://doi.org/10.1103/PhysRevLett.88.054301

Laporte-Fauret, Q., Castelle, B., Marieu, V., Bujan, S., Michalet, R., & Rosebery, D. (2020). Coastal dune morphology evolution combining Lidar and UAV surveys, Truc Vert beach 2011-2019. *Journal of Coastal Research*, *95*(sp1), 163–167. https://doi.org/10.2112/SI95-032.1

Moore, L. J., Goldstein, E. B., Vinent, O. D., Walters, D., Kirwan, M., Lauzon, R., et al. (2018). The role of ecomorphodynamic feedbacks and landscape couplings in influencing the response of barriers to changing climate. In *Barrier dynamics and response to changing climate* (pp. 305–336). Springer International Publishing. https://doi.org/10.1007/978-3-319-68086-6_10

Ollerhead, J., Davidson-Arnott, R., Walker, I. J., & Mathew, S. (2013). Annual to decadal morphodynamics of the foredune system at Greenwich Dunes, Prince Edward Island, Canada. *Earth Surface Processes and Landforms*, *38*(3), 284–298. https://doi.org/10.1002/ESP.3327

Parsons, D. R., Walker, I. J., & Wiggs, G. F. S. (2004). Numerical modelling of flow structures over idealized transverse aeolian dunes of varying geometry. *Geomorphology*, *59*(1–4), 149–164. https://doi.org/10.1016/J.GEOMORPH.2003.09.012

Poppema, D. W., Baas, A. C. W., Hulscher, S. J. M. H., & Wijnberg, K. M. (2022). Cellular automaton modelling of the effects of buildings on aeolian bedform dynamics. *Aeolian Research*, *59*, 100840. https://doi.org/10.1016/J.AEOLIA.2022.100840

Ranasinghe, R. (2020). On the need for a new generation of coastal change models for the 21st century. *Scientific Reports*, *10*(1), 2010. https://doi.org/10.1038/s41598-020-58376-x

Roelvink, D., & Costas, S. (2019). Coupling nearshore and aeolian processes: XBeach and Duna process-based models. *Environmental Modelling & Software*, *115*, 98–112. https://doi.org/10.1016/J.ENVSOFT.2019.02.010

Ruggiero, P., Hacker, S., Seabloom, E., & Zarnetske, P. (2018). The role of vegetation in determining dune morphology, exposure to sea-level rise, and storm-induced coastal hazards: A U.S. Pacific northwest perspective. In *Barrier dynamics and response to changing climate* (pp. 337–361). Springer International Publishing. https://doi.org/10.1007/978-3-319-68086-6_11

21699011, 2023, 9, Downloaded from https://agupubs.onlinelibrary.wiley.com/doi/10.1029/2023JF007080 by Cochrane Portugal, Wiley Online Library on [06/11/2023]. See the Terms and Conditions (https://onlinelibrary.wiley.com/terms-and-conditions) on Wiley Online Library for rules of use; OA articles are governed by the applicable Creative Commons License

Sallenger, A. H. J. (2000). Storm impact scale for barrier islands. *Journal of Coastal Research*, *16*(3), 890–895.

Schwarz, C., van Starrenburg, C., Donker, J., & Ruessink, G. (2020). Wind and sand transport across a vegetated foredune [Dataset]. Zenodo. https://doi.org/10.5281/ZENODO.4270358

Schwarz, C., van Starrenburg, C., Donker, J., & Ruessink, G. (2021). Wind and sand transport across a vegetated foredune slope. *Journal of Geophysical Research: Earth Surface*, *126*(1), e2020JF005732. https://doi.org/10.1029/2020JF005732

Smith, A. B., Jackson, D. W. T., & Cooper, J. A. G. (2017). Three-dimensional airflow and sediment transport patterns over barchan dunes. *Geomorphology*, *278*, 28–42. https://doi.org/10.1016/J.GEOMORPH.2016.10.025

Stallins, J. A., & Corenblit, D. (2018). Interdependence of geomorphic and ecologic resilience properties in a geographic context. *Geomorphology*, *305*, 76–93. https://doi.org/10.1016/j.geomorph.2017.09.012

Talavera, L., Costas, S., & Ferreira, Ó. (2022). A new index to assess the state of dune vegetation derived from true colour images. *Ecological Indicators*, *137*, 108770. https://doi.org/10.1016/J.ECOLIND.2022.108770

TDS Catalog. (2022). TDS catalog [Dataset]. Retrieved from https://chlthredds.erdc.dren.mil/thredds/catalog/frf/catalog.html

Walker, I. J., Davidson-Arnott, R. G. D., Bauer, B. O., Hesp, P. A., Delgado-Fernandez, I., Ollerhead, J., & Smyth, T. A. G. (2017). Scale-dependent perspectives on the geomorphology and evolution of beach-dune systems. *Earth-Science Reviews*, *171*, 220–253. https://doi.org/10.1016/j.earscirev.2017.04.011

Walker, I. J., Hesp, P. A., Davidson-Arnott, R. G. D., Bauer, B. O., Namikas, S. L., & Ollerhead, J. (2009). Responses of three-dimensional flow to variations in the angle of incident wind and profile form of dunes: Greenwich Dunes, Prince Edward Island, Canada. *Geomorphology*, *105*(1–2), 127–138. https://doi.org/10.1016/J.GEOMORPH.2007.12.019

Walker, I. J., Hesp, P. A., Davidson-Arnott, R. G. D., & Ollerhead, J. (2006). Topographic steering of alongshore airflow over a vegetated foredune: Greenwich Dunes, Prince Edward Island, Canada. *Journal of Coastal Research*, *22*(5), 1278–1291. https://doi.org/10.2112/06A-0010.1

21699011, 2023, 9, Downloaded from https://agupubs.onlinelibrary.wiley.com/doi/10.1029/2023JF007080 by Cochrane Portugal, Wiley Online Library on [06/11/2023]. See the Terms and Conditions (https://onlinelibrary.wiley.com/terms-and-conditions) on Wiley Online Library for rules of use; OA articles are governed by the applicable Creative Commons License